DM Results from ATLAS

Hot off the press

Amanda Steinhebel
On behalf of the ATLAS Collaboration

University of Oregon

28 April 2020

Overview

Much work has been devoted to the analysis of the impressive LHC Run-2 *pp* dataset

ATLAS-CONF-2020-008

ATLAS-CONF-2020-004

ATL-PHYS-PUB-2020-007

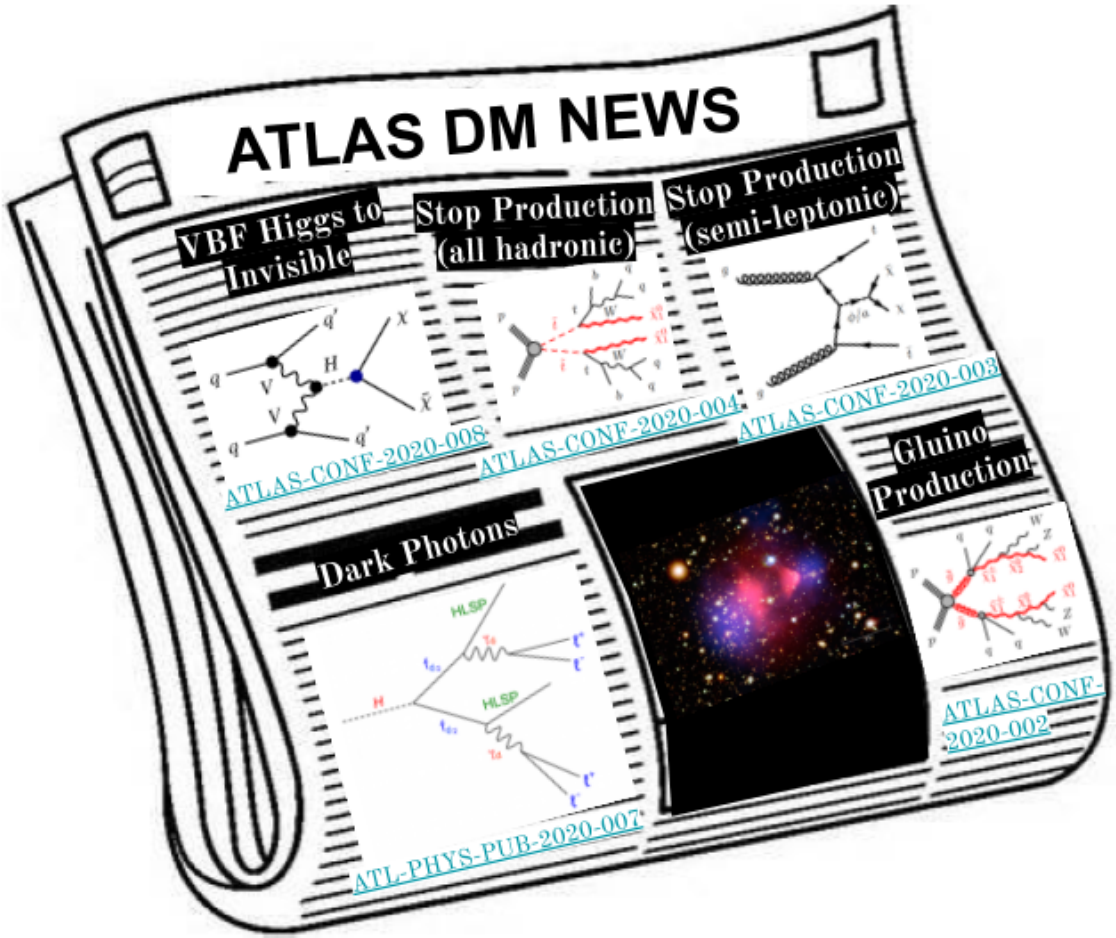

ATLAS-CONF-2020-003

ATLAS-CONF-2020-002

ATLAS and Data Collection

- Hermetic detector with nearly 4π solid angle coverage of IP
- 2-tier trigger system filters 40 MHz pp collisions to 1.5 kHz
- Run-2 data set $= 139$ fb^{-1} of $\sqrt{s} = 13$ TeV pp collisions
- 94% recording efficiency, 95.6% data quality acceptance

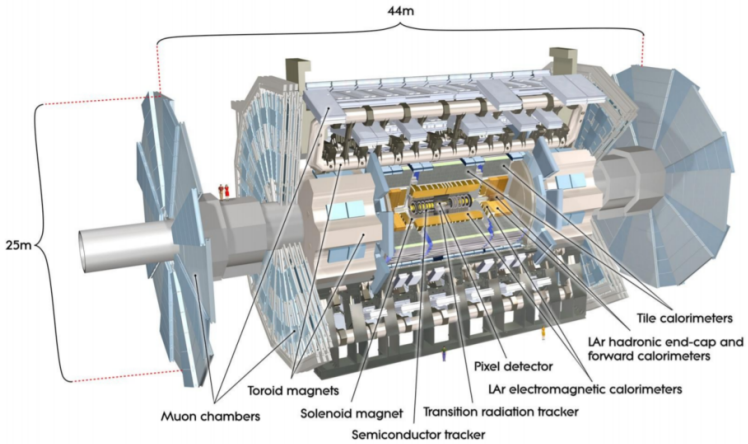

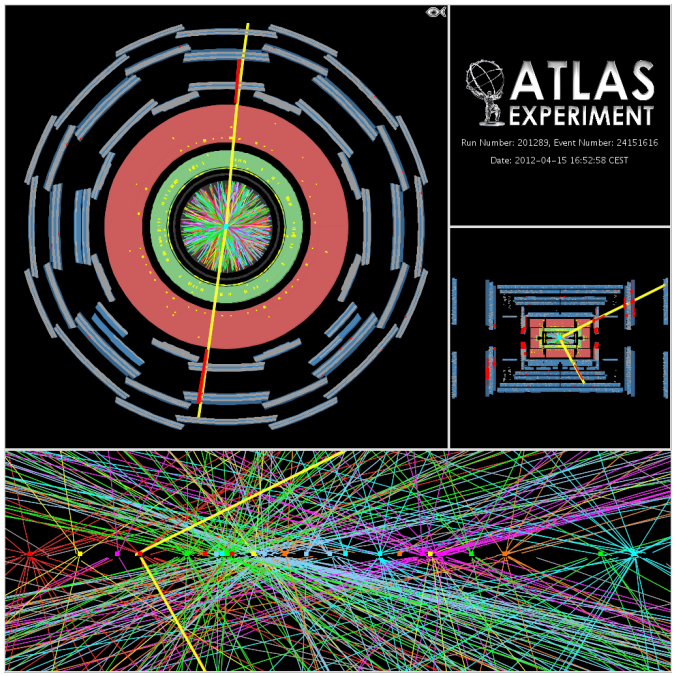

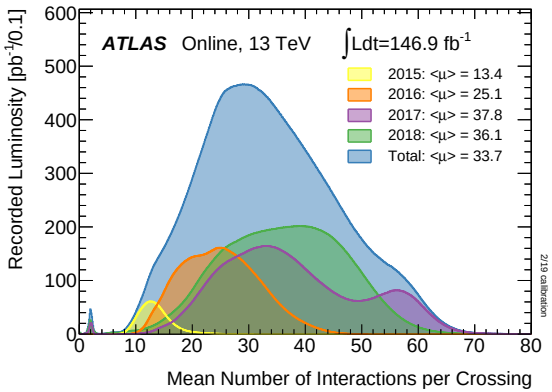

Data Quality

VBF Higgs to Invisible

- Higgs = portal between SM and DM
- Collider search complements direct DM detection
- Direct probe of $\mathcal{B}_{H\to\text{inv.}}$
  - SM-predicted 0.12%
  - Best ATLAS limit from combination: $\mathcal{B}_{H\to\text{inv.}} < 0.26(0.17)$ obs (exp) Phys. Rev. Lett. 122, 231801 (2019)
- VBF offers distinctive jets + E_T^{miss} topology

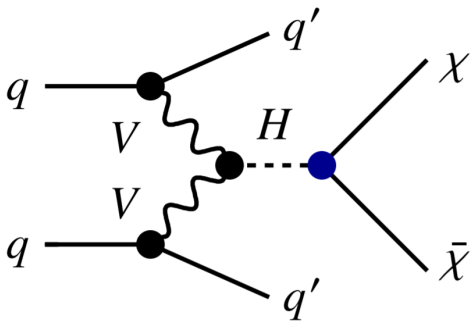

Dominant background = V+jets (95% of backgrounds)

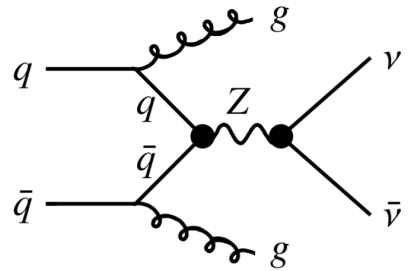

- Strong (order α_{EW}^2) VBF Z+jets

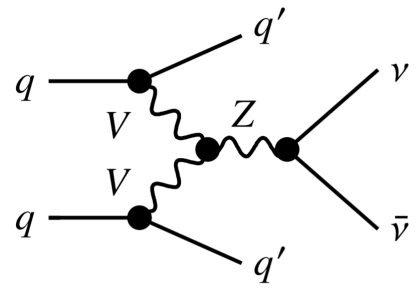

- Electroweak (order α_{EW}^4) VBF Z+jets

Selection Improvements

- Improved lepton veto: $W \to \ell\nu$ 48% $\to$ 33% of total background
- Looser kinematic requirements: $\Delta\phi_{jj} < 1.8 \to 2$, $m_{jj} > 1 \to 0.8$ TeV
- Pileup discrimination: forward jet vertex tagging and jet timing
- Optimized signal region binning: 3 $\to$ 11

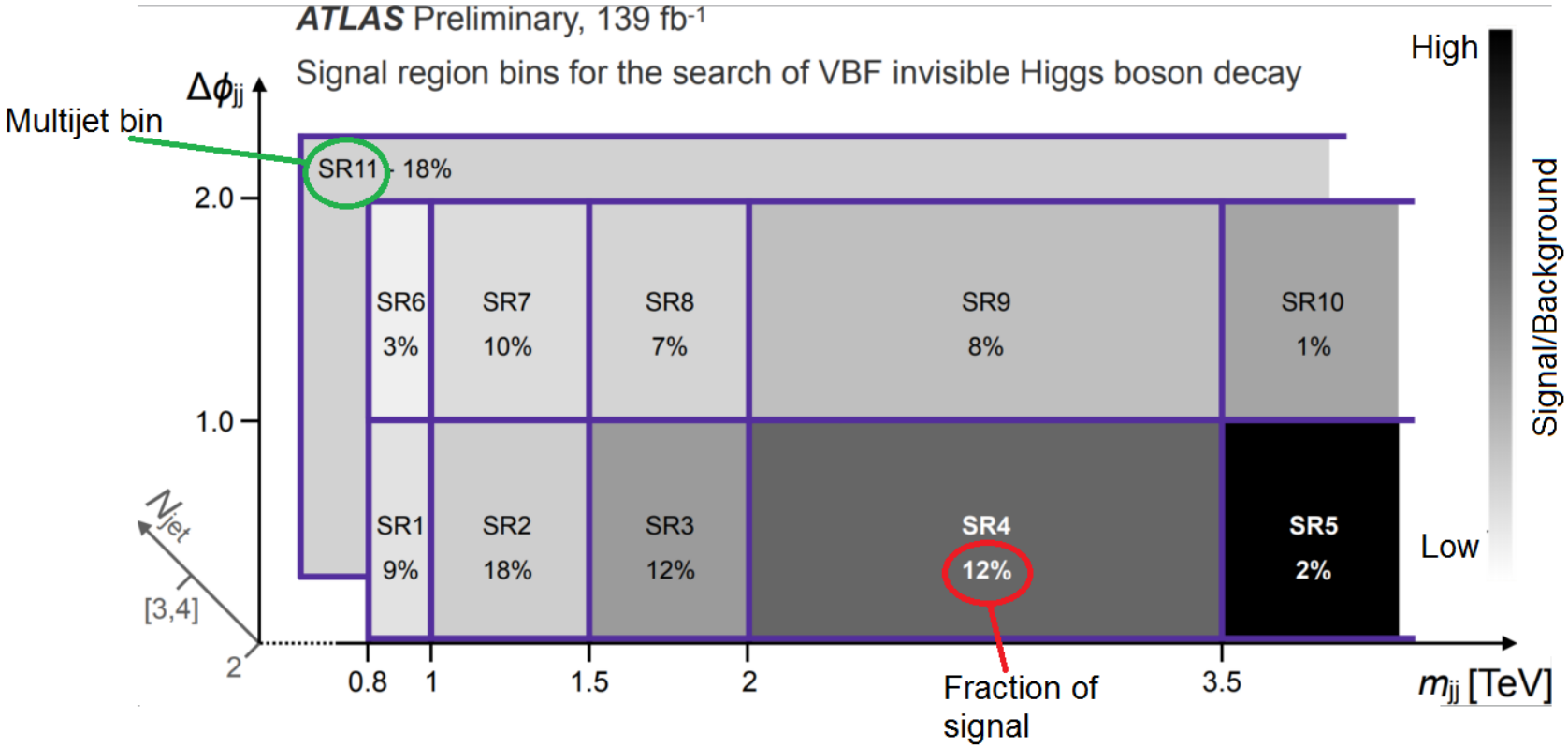

Backgrounds

- Simultaneous maximum likelihood fit of backgrounds to data in all signal and control regions
- QCD multijet predicted from data-driven method
- $t\bar{t}$, multi-boson predicted directly from simulation
- Fake electrons normalized by data from control regions

Dominant V+jets extrapolated from control regions (same as signal region with visible leptons, lepton vectorially added to E_T^{miss})

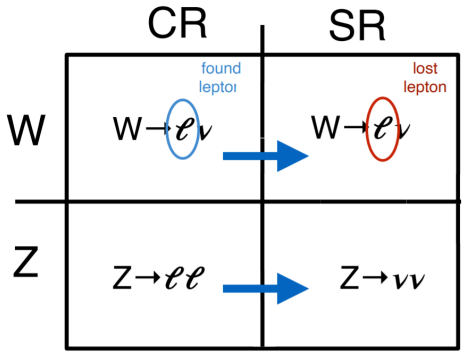

$$B_{W,i}^{\mathrm{SR}} = B_{W,i}^{\mathrm{SR,MC}} \cdot \overbrace{\frac{N_i^{W\,\mathrm{CR}} - B_{\text{non-}W,i}^{W\,\mathrm{CR}}}{B_{W,i}^{W\,\mathrm{CR,\,MC}}}}^{\text{Normalisation } \beta_{W,i}}$$

$$B_{Z,i}^{\mathrm{SR}} = B_{Z,i}^{\mathrm{SR,MC}} \cdot \underbrace{\frac{N_i^{Z\,\mathrm{CR}} - B_{\text{non-}Z,i}^{Z\,\mathrm{CR}}}{B_{Z,i}^{Z\,\mathrm{CR,\,MC}}}}_{\beta_{Z,i}}.$$

Fit for normalization factors (β_W, β_Z) in each bin

Results

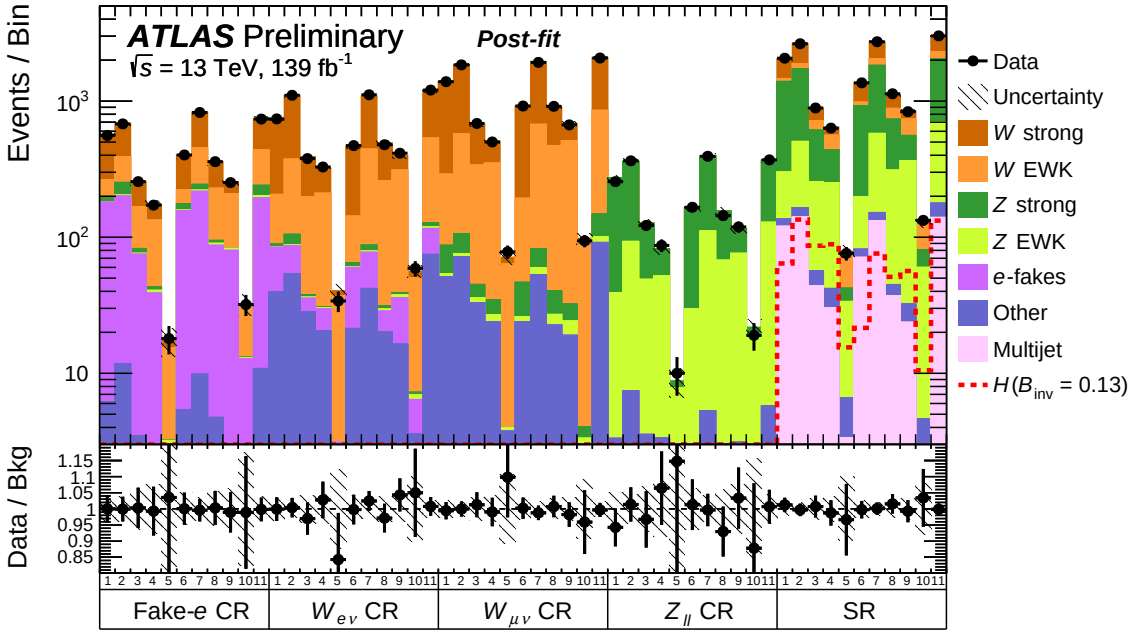

Expected and observed limits on $\mathcal{B}_{H\to\text{inv.}}$ for a 125 GeV Higgs boson

$$0.132\,(0.132^{0.183}_{0.095})\ \text{obs (exp)}$$

Previous VBF result:

$$0.37\,(0.28^{0.39}_{0.20})\ \text{obs (exp)}$$

Analysis complementary to DM direct detection experiments

Upper limits on the spin-independent WIMP–nucleon cross section using Higgs portal interpretations of $\mathcal{B}_{H\to\text{inv.}}$ at 90% CL vs. m_{WIMP}.

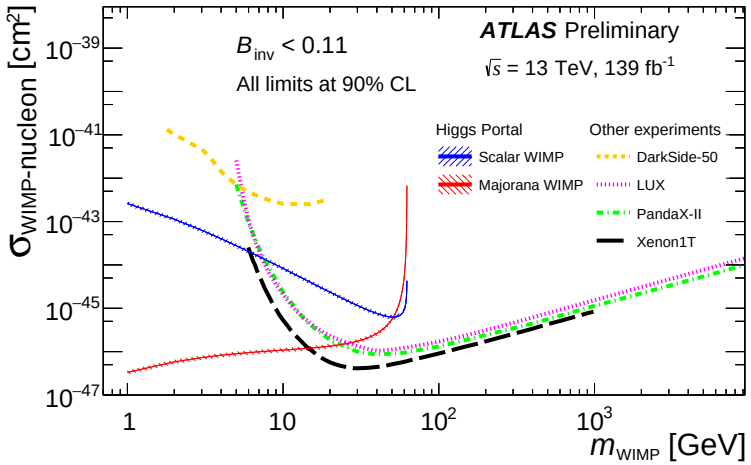

All-Hadronic Stop Search

- Interpret lightest supersymmetric particle (LSP) ($\tilde{\chi}_1^0$) as DM
- Employ soft b-tagging (for jets constructed from inner detector tracks) down to 15 GeV
- First all-hadronic 4-body decay consideration in ATLAS (below)

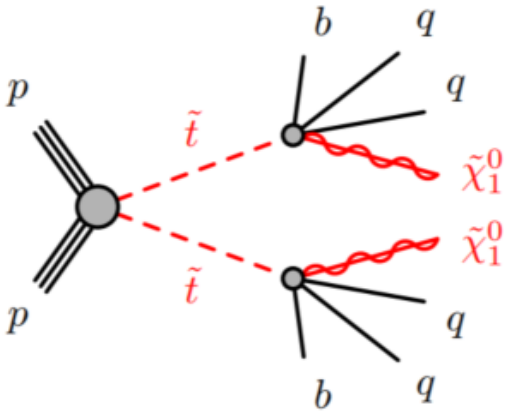

(c) $\tilde{t} \to t^* \tilde{\chi}_1^0 \to bW^* \tilde{\chi}_1^0 \to bff' \tilde{\chi}_1^0$

- Signal region sets designed to target different decays (14 SRs)
- Main backgrounds: $Z(\to \nu\nu) + \text{heavy flavor}$, $t\bar{t}$, $W + \text{jets}$, single top
- Background contributions extrapolated from control regions

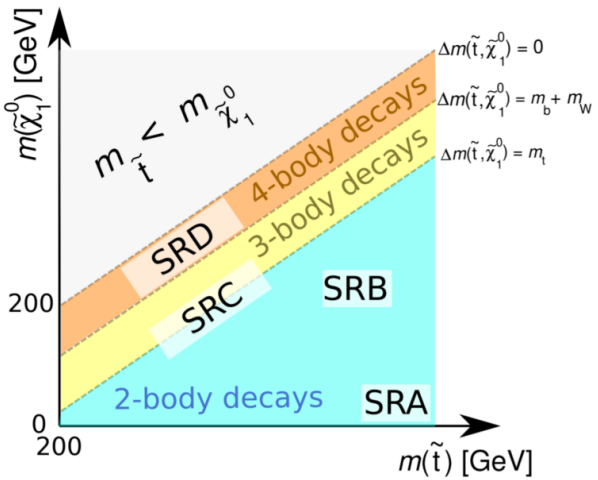

All-Hadronic Results

Backgrounds determined separately for each set of SRs with background-only fits

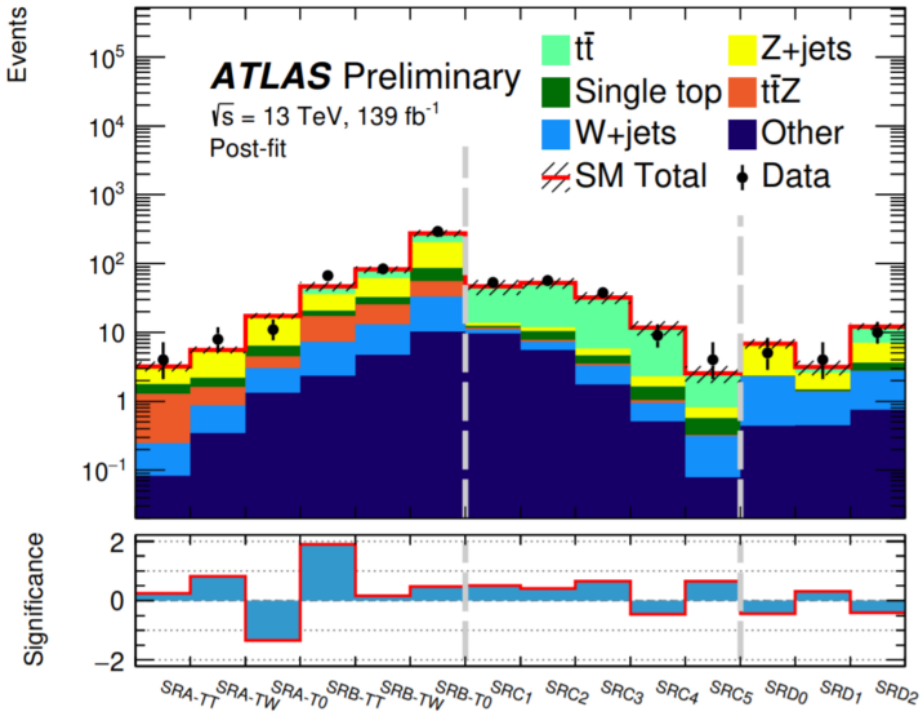

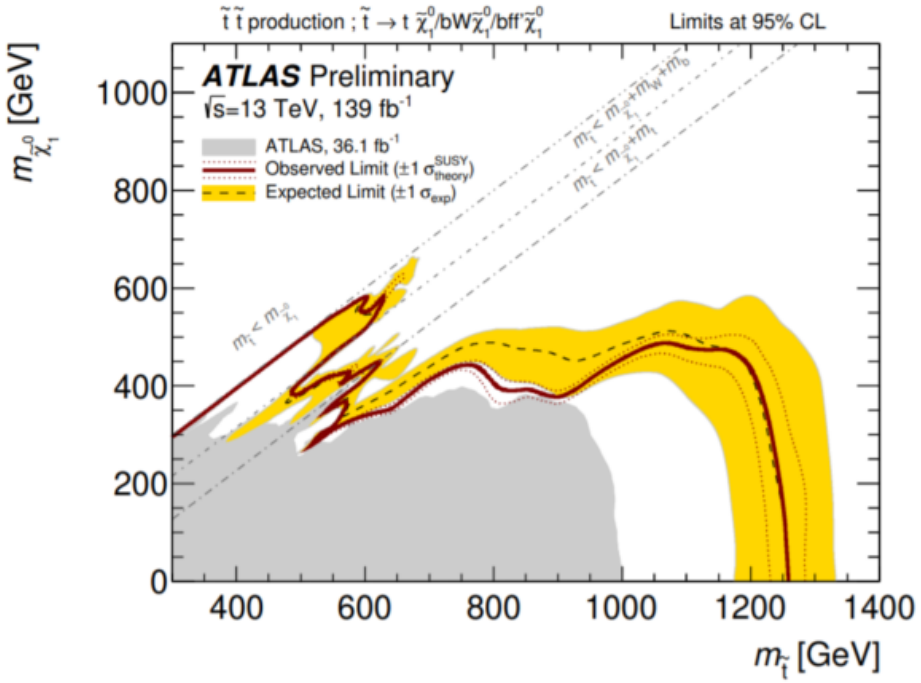

SR fit configuration with the best expected limit chosen for each signal point

Top squarks up to 1.25 TeV excluded for $m_{\tilde{\chi}^0} < 200$ GeV

Semi-Leptonic Stop Search

- Interpret LSP ($\tilde{\chi}_1^0$) as DM
- Region specific for $t\bar{t}$+spin-0 mediator decaying to DM
- Binned in $\Delta\phi(\vec{p}_T^{miss}, \ell)$
- Main backgrounds = $t\bar{t}$, $t\bar{t} + Z(\to \nu\nu)$, $W + \text{jets}$, Wt

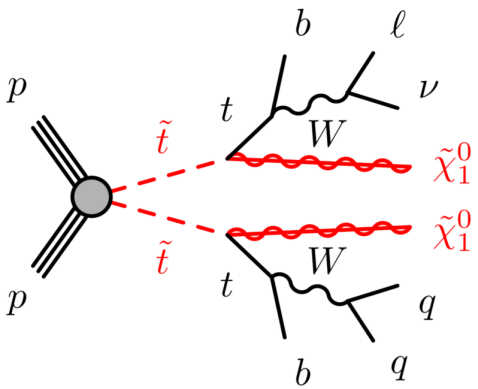

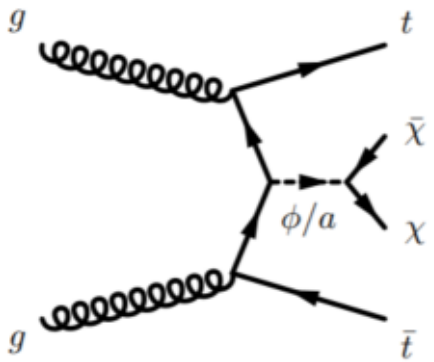

ϕ/a = (pseudo)scalar mediator

- Dileptonic $t\bar{t}$ (with lost lepton) discrimination with topness (how well event can be reconstructed as dileptonic top - likelihood method)
- Data in control regions used to constrain normalization:

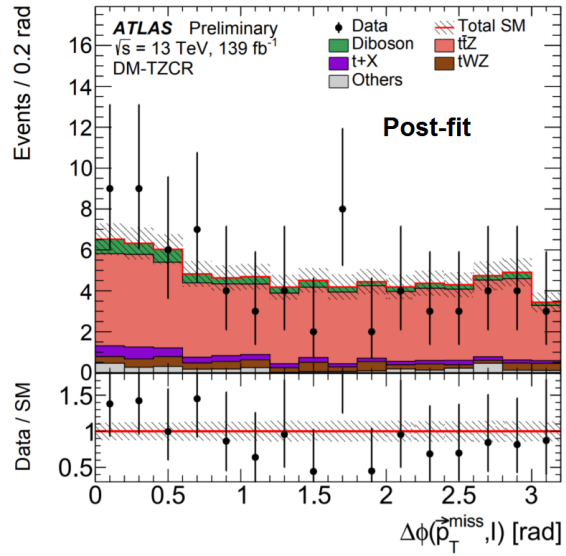

Semi-Leptonic Results

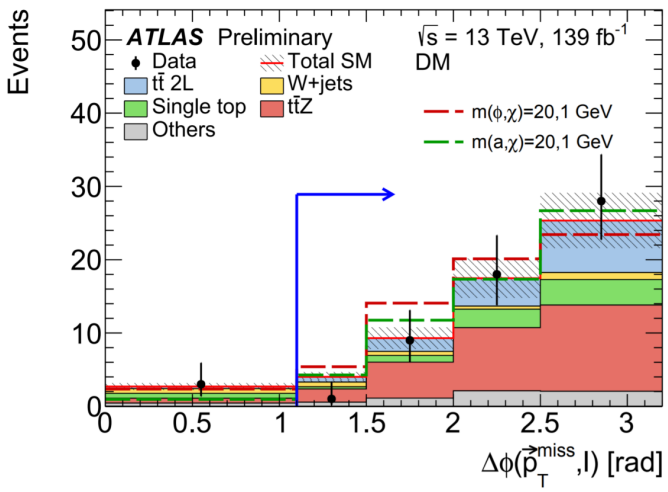

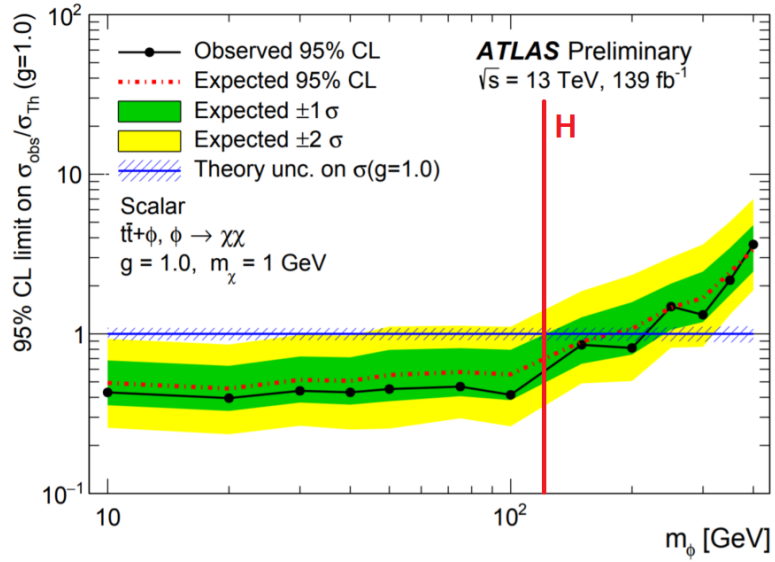

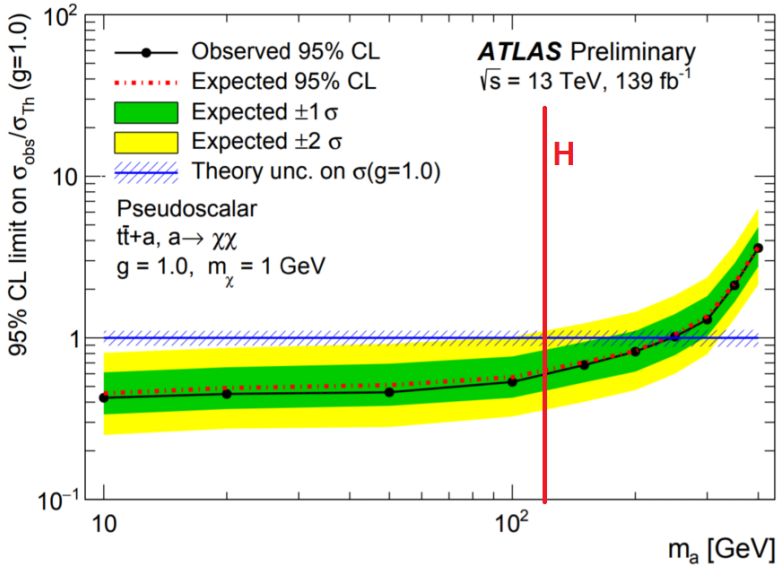

Postfit signal region, benchmark models

Assuming $m_{DM} = 1$ GeV,

Common Coupling* (g)	95% CL Excluded med. mass [GeV]
1.0	∼200
0.8	100
0.7	10

*$g = g_q = g_{DM}$

Gluino Production

- R-Parity conserving 2-step cascade models leave LSP neutralinos ($\tilde{\chi}_1^0$)
- Improved performance with Particle Flow jets and object-based MET-significance
- Large-radius ($R = 1.0$) jet multiplicities define signal regions, binned in mass of total jet system

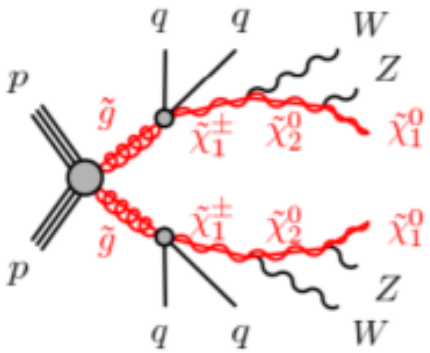

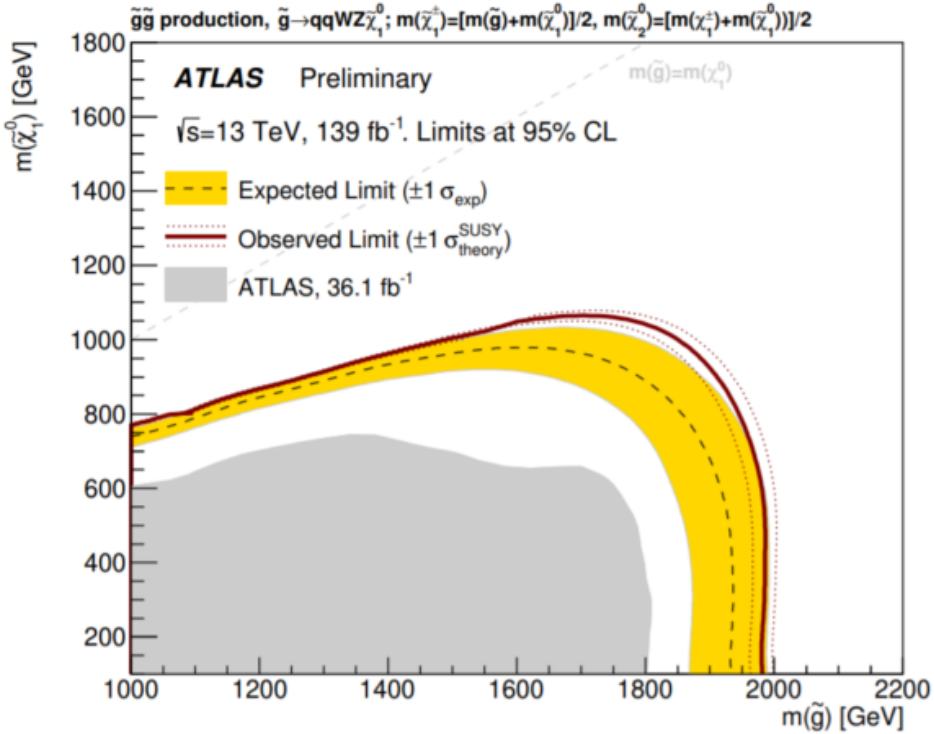

Gluinos up to ~ 2 TeV excluded for $m_{\tilde{\chi}^0} < 600$ GeV

Dark Photons

- Intersect world of DM and Long Lived Particles
  - Original work - displaced jets in hadronic calorimeter
  - Utilize Machine Learning on detector-level variables to discriminate signal and background
  - Analysis reinterpreted with RECAST
- Kinetic mixing of dark/SM γ
- Models have 2 or 4 dark photons

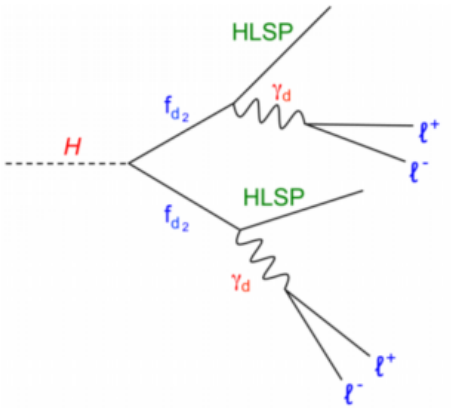

HLSP = hidden LSP
f_d = dark fermion
γ_d = dark photon (to light SM f)

First constraints set for $m_H = 125$ GeV

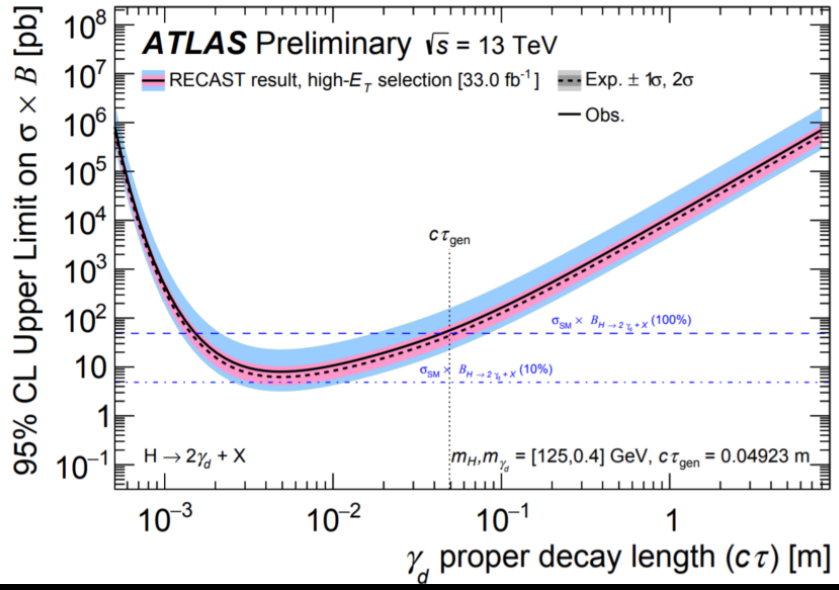

Conclusion

The lack of beams and access to CERN has not stifled the release of exciting results!

- VBF Higgs to Invisible
  - Strictest limit on $\mathcal{B}_{H\to\text{inv.}}$ by a single channel - 0.13(0.13) obs (exp)
  - ATLAS-CONF-2020-008
- All-Hadronic Stop Search
  - Top squarks up to 1.25 TeV excluded for $m_{\tilde{\chi}^0} < 200$ GeV
  - ATLAS-CONF-2020-004
- Semi-Leptonic Stop Search
  - Exclude (pseudo)scalar mediator (SM→DM) masses below 200 GeV for $m_{DM} = 1$ GeV
  - ATLAS-CONF-2020-003
- Dark Photons
  - RECAST analysis, first constraints on γ_d $c\tau$ from m_H
  - ATL-PHYS-PUB-2020-007
- Gluino Production
  - Gluinos up to ~ 2 TeV excluded for $m_{\tilde{\chi}^0} < 600$ GeV
  - ATLAS-CONF-2020-002

Backup Slides

VBF Higgs to Invisible

Contribution to $\mathcal{B}_{H\to\text{inv.}}$

13 TeV Cross sections for 125.0 GeV Higgs

Channel	XS [pb]
ggF	43.92
VBF	3.748
WH	1.380
ZH	0.8696
ttH	0.5085
bbH	0.5116

$$\frac{\sigma_{ggF}(H+\text{jet})}{\sigma(Z+\text{jet})\cdot\text{BR}(Z\to\nu\nu)} \sim \frac{1}{300}$$

$$\frac{\sigma_{VBF}(H+qq)}{\sigma(Z+\text{jet})\cdot\text{BR}(Z\to\nu\nu)} \sim \frac{4}{3}$$

VBF not largest XS but most sensitive channel to measure $\mathcal{B}_{H\to\text{inv.}}$ Drives combination

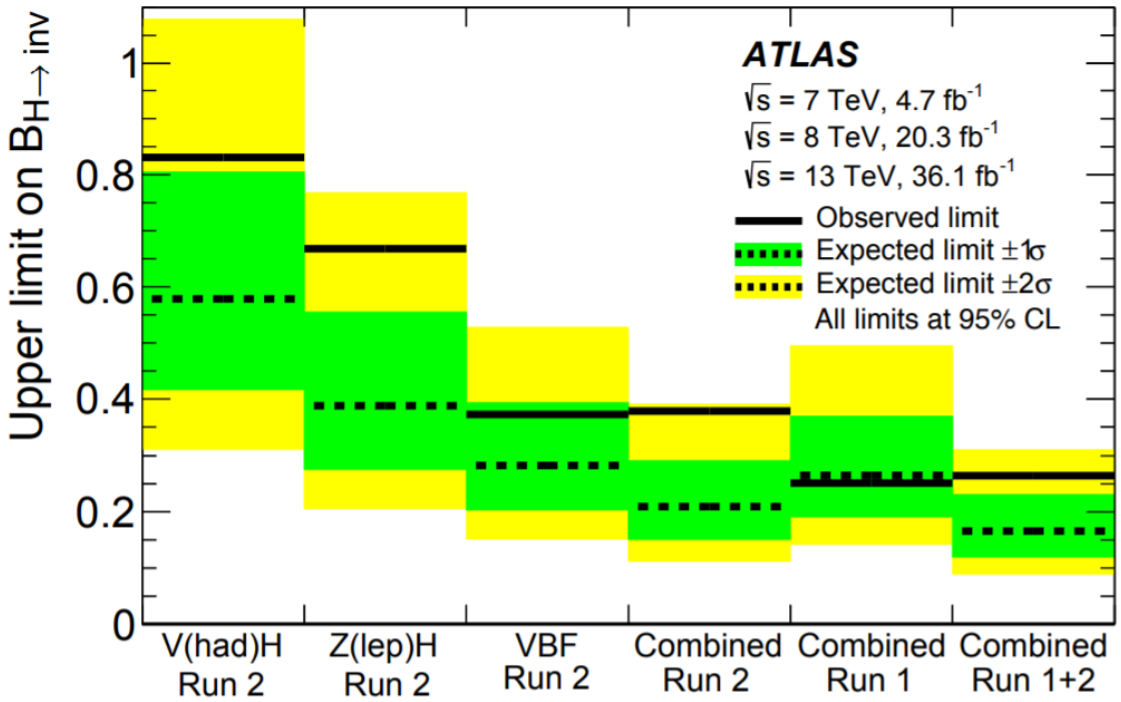

Phys. Rev. Lett. 122, 231801 (2019)

Evolution of VBF $\mathcal{B}_{H\to\text{inv.}}$ Limits

Limit setting conducted at 95% CL

Limit	Bins	Observed	Expected
Run-1 Paper (JHEP 01 (2016) 172)	3	0.28	0.31
36 fb^{-1} Paper (Phys. Lett. B 793 (2019) 499)	3	0.37	0.28
Full Run-2 (ATLAS-CONF-2020-008)	11	0.132	0.132

Object Definitions (See twiki)

Object	Requirement
e(μ) Veto	4.5(4) GeV Loose (Loose) $\|\eta\| < 2.47$ include crack (2.7)
e(μ) CR	7(7) GeV Tight (Medium) $\|\eta\| < 2.47$ exclude crack (2.5)
Photon	20 GeV Tight $\|\eta\| < 2.37$ (exclude crack)
Jets	Anti-k_T 0.4 PFlow (fJVT copied from EMTopo) 25 GeV $\|\eta\| < 4.5$ JVT>0.59 if $p_T > 60$ GeV and $\|\eta\| < 2.5$ Leading 2 - fJVT< 0.5&&$\|$JetTiming$\| < 11$ns
MET	Loose

Overlap Removal

Table 2: Overview of the overlap removal between objects and the corresponding matching criteria, listed according to priority.

Remove	Keep	Matching criteria
electron	electron	shared inner detector track, $p_{\mathrm{T}}^{\mathrm{electron1}} < p_{\mathrm{T}}^{\mathrm{electron2}} \Rightarrow$ remove electron 1
muon	electron	muon with calorimeter deposits and shared inner detector track
electron	muon	shared inner detector track
photon	electron	$\Delta R < 0.4$
photon	muon	$\Delta R < 0.4$
jet	electron	$\Delta R < 0.2$
electron	jet	$\Delta R < \min(0.4, 0.04 + 10\,\mathrm{GeV}/p_{\mathrm{T}}^{e})$
jet	muon	number of tracks < 3 and $\Delta R < 0.2$
muon	jet	$\Delta R < \min(0.4, 0.04 + 10\,\mathrm{GeV}/p_{\mathrm{T}}^{\mu})$
photon	jet	$\Delta R < 0.4$

Signal Region Definitions

Lepton/photon veto	$E_T^{miss} > 200$ GeV	$\|\Delta\phi_{jj}\| < 2.0$
$p_T(j_1) > 80$ GeV	$^*H_T^{miss} > 180$ GeV	$\|\Delta\eta_{jj}\| > 3.8$
$p_T(j_2) > 50$ GeV	$E_T^{soft} < 20$ GeV	$m_{jj} > 0.8$ TeV
$\eta(j_1) \cdot \eta(j_2) < 0$	$2 \leq N_{jet} \leq 4$	$N_b < 2$
$p_T(j) > 25$ GeV	|jet timing| < 11 ns	fJVT$< 0.5(0.2)$ when
MET Triggers	Med. JVT WP	$E_T^{miss} > (<)180$ GeV

If $N_{jet} > 2$,
Centrality $C_i < 0.6$
$m_i^{rel} < 0.05$

Centrality $C_i = \exp\left(-\frac{4}{(\eta_1-\eta_2)^2}\left(\eta_i - \frac{\eta_1+\eta_2}{2}\right)^2\right)$
$m^{rel} = \frac{\max M_{j_3 j}}{M_{jj}}$

Control regions for V+jets defined identically except for lepton requirements (See Backup 22)

* H_T^{miss} = vectoral sum of all jet p_T if $p_T > 20$ GeV, including pile-up jets (no JVT requirement)

Control Region Definitions

Lepton triggers (e), OR'ed with MET triggers (μ)
Same requirements as SR, except...

Cut Name	$W \to e\nu$	$W \to \mu\nu$	$Z \to \ell^-\ell^+$
	CR1L (WCR)		CR2L (ZCR)
Selected leptons	$e^{\pm}$	$\mu^{\pm}$	ℓ^-, ℓ^+
$p_T(\ell_1)$	> 30 GeV	> 30 GeV	> 30 GeV
$p_T(\ell_2)$	–	–	> 7 GeV
$\lvert M(\ell\ell) - M_Z \rvert$	–	–	< 25 GeV
E_T^{miss} (with leptons)	–	–	< 70 GeV
S_{MET}	> 4.0 GeV$^{1/2}$	–	–

$$\text{event-based } S_{\mathrm{MET}} = \frac{E_T^{miss}}{\sqrt{p_T^{j1}+p_T^{j2}+p_T^{e}}}$$

$W_{e\nu}$ anti-ID CR

For mis-identified electrons in the $W_{e\nu}$ CR, use additional CR enriched with fake electrons to derive scaling factor

Background accounts for $\sim 3\%$ of $W_{e\nu}$ CR

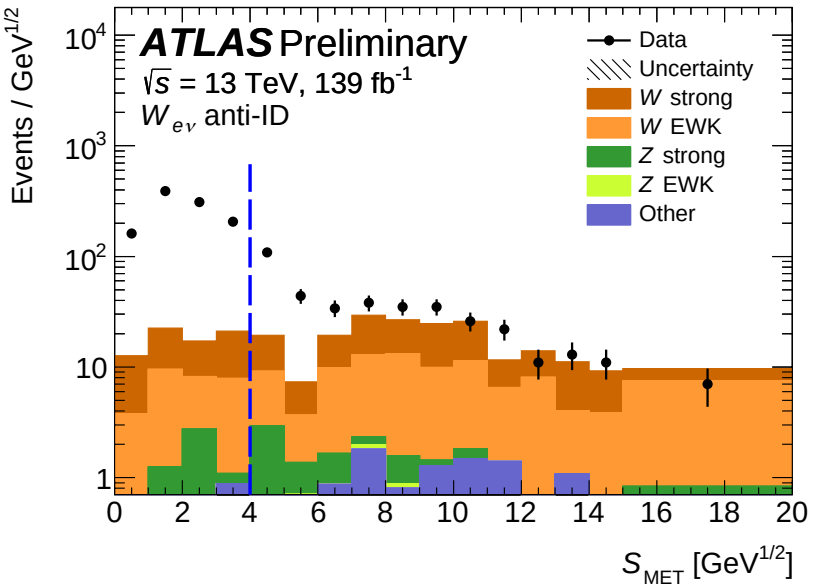

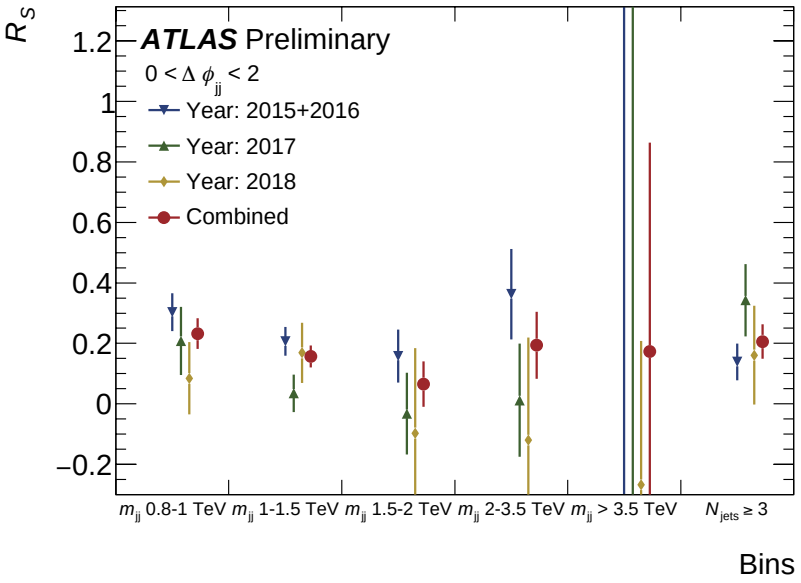

QCD Multijet Estimate

Jet mis-measurement from JER, experimental effects, PU, mis-tagging can lead to fake E_T^{miss} and signal-like topologies

use data-driven estimation technique

variation of "Rebalance and Smear"

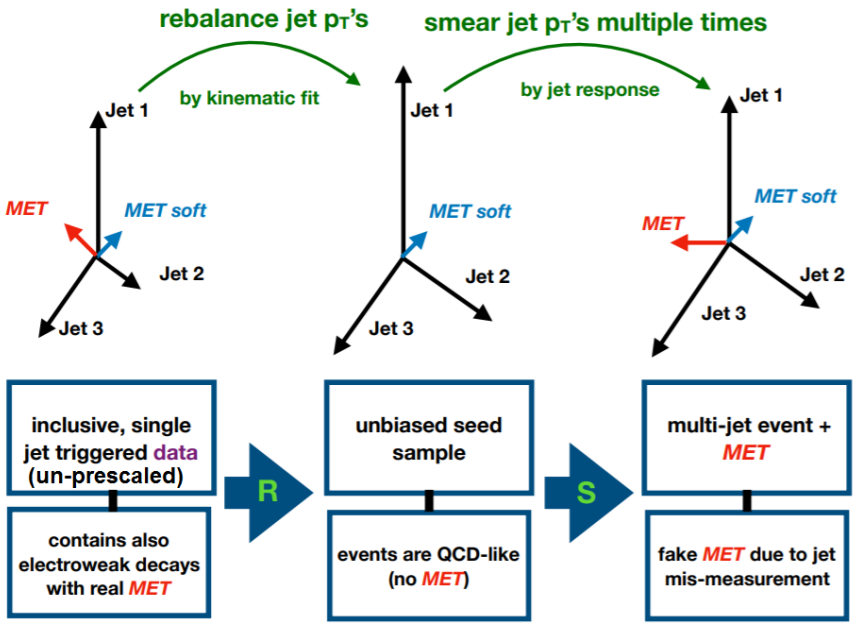

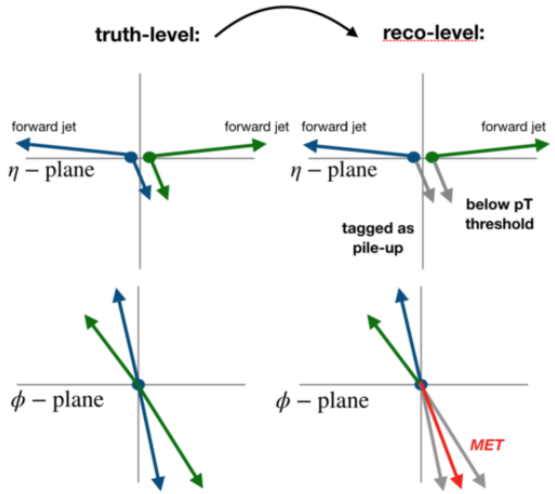

QCD Rebalance and Smear (R&S) Procedure

1. Identify jets from single jet triggered events (lepton veto) as hard scatter (HS) or pile up (PU) based on (f)JVT
2. Rebalance HS and PU collections separately by adjusting momenta (within uncertainties) until E_T^{miss} is eliminated
3. Smear within jet response templates
4. Merge collections and reevaluate (f)JVT
5. Split events into those with only HS jets or a combination of HS+PU
6. Normalize separately using MJ CR
7. Apply trigger-efficiency correction
8. Merge and normalize full distribution in low-m_{jj} ($200 < m_{jj} < 800$ GeV) and low-E_T^{miss} ($100 < E_T^{miss} < 150$ GeV, $H_T^{miss} > 100$ GeV) CRs

V+jets Uncertainties

- On-the-fly SHERPA MC variations of factorisation and renormalisation scales - use envelope of 7 variations
- Fractional uncertainty of strong (EWK) from $\frac{+27\%}{-18\%}\left(\frac{+11\%}{-9\%}\right) \rightarrow \frac{+43\%}{-26\%}\left(\frac{+29\%}{-20\%}\right)$ from low$\rightarrow$ high m_{jj}
- Correlated uncertainties cause cancellation between SR and corresponding CR; no correlation between strong and EWK or W and Z processes
- Resummation and CKKW varied and applied as reweighting factors binned in p_T^V and $N_{true\ jets}$
- Relative errors for resummation (CKKW) range from 4% (4%) to 8% (6%)
- PDF uncertainties range from 1% to 2%

Results - Post-fit Distributions

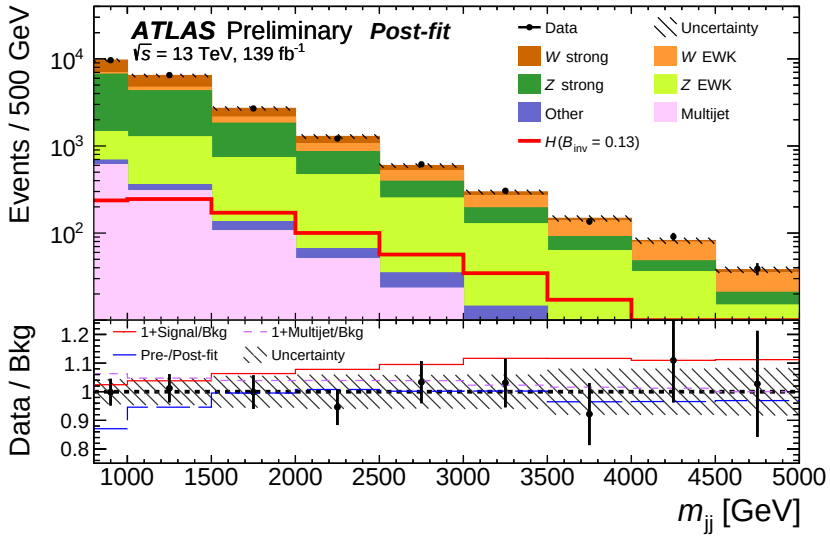

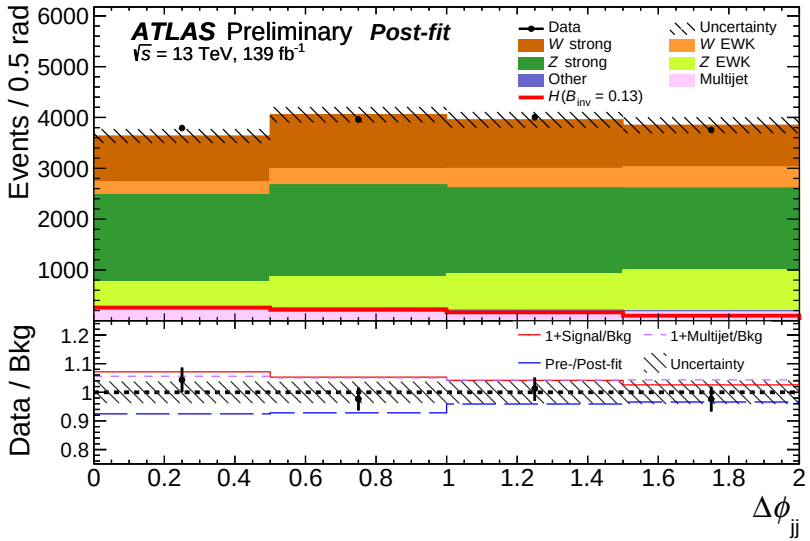

Relative impact Δ of the 95% CL upper limit on $\mathcal{B}_{\text{inv}}$ if a group of uncertainties is "removed", i.e. if the corresponding nuisance parameters are fixed to their best fit values.

Source	Δ [%]
Jet energy scale	1.8
JER	5.5
Lepton	4.6
Other	1.9
Multijet	7.0
V+jets Theory	1.6
Signal Theory	1.0
MC Stats	7.9
Data Stats	17.3

Data is consistant with background-only hypothesis

Interpretation - Heavy Scalar $\rightarrow$ Inv.

Improvement at higher scalar mediator mass due to better S/B

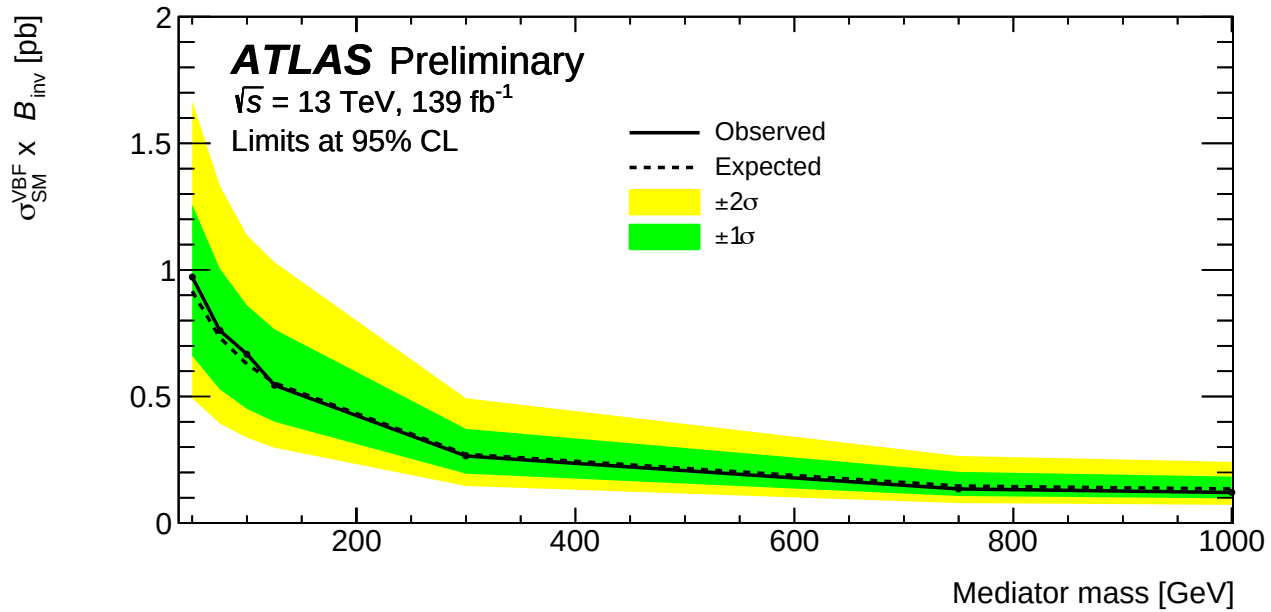

Figure 11: Upper limit on cross section times branching ratio to invisible particles for heavy scalar mediator particle as a function of its mass.

95% CL upper limit on $\sigma^{VBF} \times \mathcal{B}_{H\rightarrow \text{inv.}}$ ranges from 0.97 pb (50 GeV mediator mass) to 0.12 pb (1 TeV mediator mass)

$t\bar{t}+E_T^{miss}$

All-Hadronic Stop

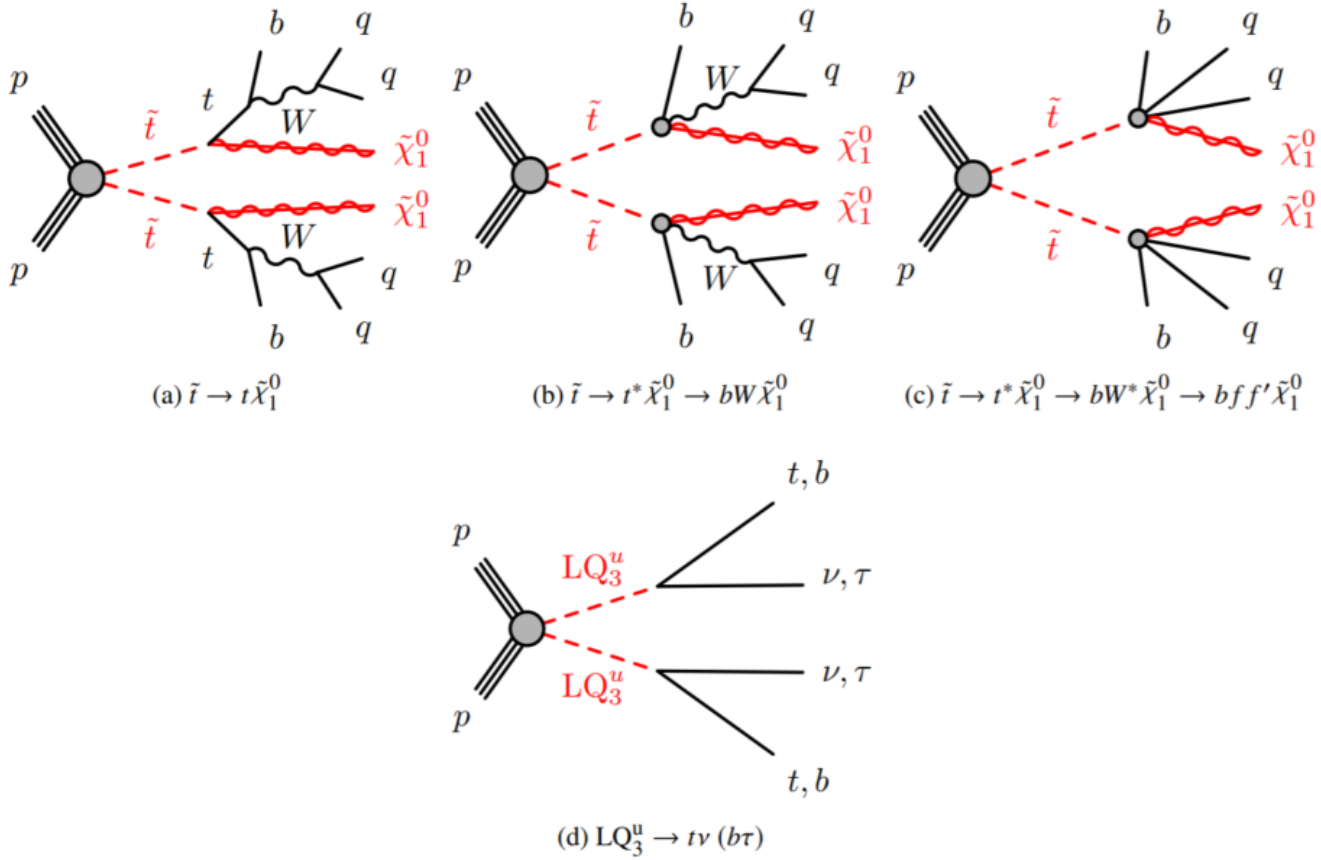

LSP = lightest neutralino ($\tilde{\chi}_1^0$), interpreted as DM

Two-, three-, and four-body squark decays

d) up-type, third-generation scalar leptoquark pair production

All-Hadronic SRA-B

Variable/SR	SRA-TT	SRA-TW	SRA-T0	SRB-TT	SRB-TW	SRB-T0
Trigger	$E_{\mathrm{T}}^{\mathrm{miss}}$					
$E_{\mathrm{T}}^{\mathrm{miss}}$	> 250 GeV					
N_{ℓ}	exactly 0					
N_{j}	≥ 4					
$p_{\mathrm{T},2}$	> 80 GeV					
$p_{\mathrm{T},4}$	> 40 GeV					
$\lvert\Delta\phi_{\mathrm{min}}\left(\mathbf{p}_{\mathrm{T},1-4}, \mathbf{p}_{\mathrm{T}}^{\mathrm{miss}}\right)\rvert$	> 0.4					
N_b	≥ 2					
$m_{\mathrm{T}}^{b,\mathrm{min}}$	> 200 GeV					
τ-veto	✓					
$m_1^{R=1.2}$	> 120 GeV					
$m_2^{R=1.2}$	> 120 GeV	$60 - 120$ GeV	< 60 GeV	> 120 GeV	$60 - 120$ GeV	< 60 GeV
$m_1^{R=0.8}$	> 60 GeV			–		
$j_1^{R=1.2}(b)$	✓			–		
$j_2^{R=1.2}(b)$	✓	–				
$\Delta R\,(b_1, b_2)$	> 1.0	–		> 1.4		
$m_{\mathrm{T}}^{b,\mathrm{max}}$	–			> 200 GeV		
$\mathcal{S}$	> 25			> 14		
m_{T2,χ^2}	> 450 GeV			< 450 GeV		

All-Hadronic SRC, SRD

$$R_{ISR} \equiv \frac{E_T^{\text{miss}}}{p_T^{\text{ISR}}} \sim \frac{m_{\tilde{\chi}_1^0}}{m_{\tilde{t}}}$$

Variable/SR	SRC1	SRC2	SRC3	SRC4	SRC5
Trigger	$E_{\text{T}}^{\text{miss}}$				
$E_{\text{T}}^{\text{miss}}$	> 250 GeV				
N_ℓ	exactly 0				
N_j	≥ 4				
$p_{T,2}$	> 80 GeV				
$p_{T,4}$	> 40 GeV				
N_b	≥ 2				
$E_{\text{T}}^{\text{miss,track}}$	> 30 GeV				
$\lvert\Delta\phi\left(\mathbf{p}_{\text{T}}^{\text{miss}}, \mathbf{p}_{\text{T}}^{\text{miss,track}}\right)\rvert$	$< \pi/3$				
$\lvert\Delta\phi\left(\mathbf{p}_{\text{T},1-2}, \mathbf{p}_{\text{T}}^{\text{miss}}\right)\rvert$	> 0.4				
N_j^S	≥ 4				
$p_{\text{T}}^{\text{ISR}}$	> 400 GeV				
$p_{\text{T},1}^{S,b}$	> 50 GeV				
$p_{\text{T},4}^{S}$	> 50 GeV				
m_S	> 400 GeV				
$\lvert\Delta\phi\left(\mathbf{p}_{\text{T}}^{\text{ISR}}, \mathbf{p}_{\text{T}}^{\text{miss}}\right)\rvert$	> 3.0				
R_{ISR}	0.30 – 0.40	0.40 – 0.50	0.50 – 0.60	0.60 – 0.70	> 0.70

Variable/SR	SRD0	SRD1	SRD2
Trigger	$E_{\text{T}}^{\text{miss}}$		
$E_{\text{T}}^{\text{miss}}$	> 250 GeV		
N_ℓ	exactly 0		
N_b	exactly 0	exactly 1	≥ 2
$p_{\text{T}}^{\text{j}^{\text{ISR}}}$	> 250 GeV		
$\lvert\Delta\phi\left(\mathbf{p}_{\text{T}}^{\text{j}^{\text{ISR}}}, \mathbf{p}_{\text{T}}^{\text{miss}}\right)\rvert$	> 2.4		
$E_{\text{T}}^{\text{miss,track}}$	> 30 GeV		
$\lvert\Delta\phi\left(\mathbf{p}_{\text{T}}^{\text{miss}}, \mathbf{p}_{\text{T}}^{\text{miss,track}}\right)\rvert$	$< \pi/3$		
N_b^{track}	≥ 1		–
$\lvert\Delta\phi_{\text{min}}\left(\mathbf{p}_{\text{T},1-4}, \mathbf{p}_{\text{T}}^{\text{miss}}\right)\rvert$	> 0.4	–	
$\lvert\eta_1^{b,\text{track}}\rvert$	< 1.2	–	
$\max\lvert\Delta\phi\left(\mathbf{p}_{\text{T}}^{\text{j}^{\text{ISR}}}, \mathbf{p}_{\text{T}}^{b^{\text{track}}}\right)\rvert$	> 2.2	–	
$\lvert\Delta\phi\left(\mathbf{p}_{\text{T},1}^{b^{\text{track}}}, \mathbf{p}_{\text{T},2}^{b^{\text{track}}}\right)\rvert$	< 2.5	–	
$p_{\text{T},1}^{b,\text{track}}$	< 50 GeV	> 10 GeV	–
$p_{\text{T},1}^{\text{track}}$	–	< 40 GeV	–
$\lvert\Delta\phi\left(\mathbf{p}_{\text{T},1-4}^{\text{j}^{\text{track}}}, \mathbf{p}_{\text{T}}^{\text{j}^{\text{ISR}}}\right)\rvert$	–	> 1.2	–
$\lvert\eta_1^b\rvert$	–	< 1.6	–
$\lvert\Delta\phi\left(\mathbf{p}_{\text{T}}^{\text{j}^{\text{ISR}}}, \mathbf{p}_{\text{T},1}^{b}\right)\rvert$	–	> 2.2	
$\lvert\eta_2^b\rvert$	–		< 1.2
$p_{\text{T},1}^{b}$	–		< 175 GeV
$\lvert\Delta\phi\left(\mathbf{p}_{\text{T}}^{\text{j}^{\text{ISR}}}, \mathbf{p}_{\text{T},2}^{b}\right)\rvert$	–		> 1.6
$E_{\text{T}}^{\text{miss}}/\sqrt{H_{\text{T}}}$	$> 26\sqrt{\text{GeV}}$	$> 22\sqrt{\text{GeV}}$	

All-Hadronic CRs

3 independent fits:
fit SRA-B, fit SRC, fit SRD CRs/VRs defined orthogonally for each fit, not

necessarily between fits
Kinematically similar to corresponding SR, but some cuts loosened for higher statistics

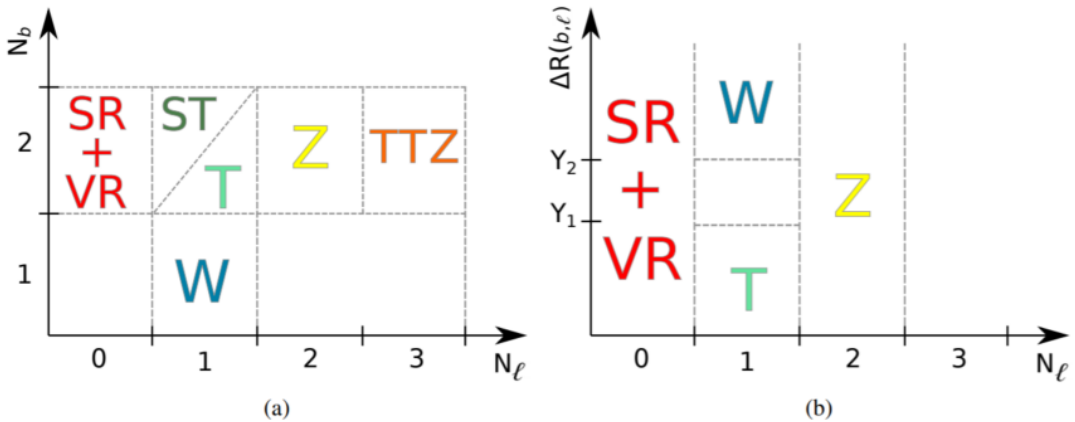

Figure 3: A summary of the background control region strategy used in the (a) SRA–B and (b) SRD fits. The orthogonality between the Z + jets (Z), $t\bar{t}$ + Z (TTZ), $t\bar{t}$ (T), W + jets (W), and single top (ST) backgrounds control regions and the signal and validation regions (SR+VR) included in the SRA–B fit rely on the number of leptons, N_ℓ, and the number of b–tagged jets, N_b. T and ST are made orthogonal by selecting either low (< 20 GeV) or high (> 27 GeV) p_T leptons, respectively. The orthogonality between the Z + jets (Z), $t\bar{t}$ (T), and W + jets (W) backgrounds control regions and the signal and validation regions (SR+VR) included in the SRD fit relies on N_ℓ and the distance between the b–tagged jet (b–tagged track jet in CRWD0) closest to the lepton, $\Delta R(b,\ell)$. The selection applied on the latter (Y_1, Y_2) varies depending on N_b. Additional selections not appearing on the sketches ensure

All-Hadronic Systematics

Table 9: Systematic uncertainties (in percent) greater than 1% for at least one category within SRA and SRB. Uncertainties are expressed relative to the total background estimates and larger uncertainties are shown with higher opacity. The uncertainties due to the scaling of background events based on data in control regions are indicated for each background component by $\mu_{t\bar{t}}$, $\mu_{t\bar{t}+Z}$, μ_Z, μ_W, and $\mu_{\text{single top}}$. The theory uncertainties quoted for each background include the different shape uncertainties described in the text.

	SRA-TT	SRA-TW	SRA-T0	SRB-TT	SRB-TW	SRB-T0
Total syst. unc.	15	12	10	14	9	9
$t\bar{t}$ theory	2	2	1	11	6	4
Single top theory	7	5	4	1	<1	1
$t\bar{t}Z$ theory	3	<1	<1	<1	<1	<1
Z theory	<1	<1	1	<1	<1	<1
$\mu_{t\bar{t}}$	<1	<1	<1	4	4	4
$\mu_{t\bar{t}+Z}$	6	2	2	4	3	1
μ_Z	3	5	5	3	3	3
μ_W	2	3	3	4	4	3
$\mu_{\text{single top}}$	6	4	5	3	4	5
JER	7	3	2	6	2	3
JES	4	4	2	2	<1	<1
b–tagging	5	3	3	2	1	2
$E_{\text{T}}^{\text{miss}}$ soft term	2	1	1	<1	<1	<1
MC statistics	7	7	5	3	3	2

Table 10: Systematic uncertainties (in percent) greater than 1% for at least one category within SRC and SRD. Uncertainties are expressed relative to the total background estimates and larger uncertainties are shown with higher opacity. The uncertainties due to the scaling of background events based on data in control regions are indicated for each background component by $\mu_{t\bar{t}}$, μ_Z, and μ_W. The theory uncertainties quoted for each background include the different shape uncertainties described in the text.

	SRC1	SRC2	SRC3	SRC4	SRC5	SRD0	SRD1	SRD2
Total syst. unc.	25	18	20	27	27	18	31	12
$t\bar{t}$ theory	20	11	12	16	21	4	9	5
Single top theory	<1	<1	<1	<1	<1	<1	4	2
Z theory	<1	<1	1	2	4	7	3	2
W theory	<1	<1	1	2	3	<1	<1	<1
$\mu_{t\bar{t}}$	12	13	14	14	11	<1	2	5
μ_Z	<1	<1	<1	<1	<1	5	3	2
μ_W	<1	<1	<1	<1	<1	4	5	3
JER	5	<1	8	15	7	8	18	4
JES	<1	1	<1	4	6	1	4	2
b–tagging	2	2	2	2	2	3	5	7
Track jet flavour	<1	<1	<1	<1	<1	4	7	<1
Track jet flavour (low p_{T})	<1	<1	<1	<1	<1	7	4	1
$E_{\text{T}}^{\text{miss}}$ soft term	<1	<1	<1	<1	3	<1	<1	<1
Pileup	<1	<1	<1	1	<1	2	12	<1
MC statistics	3	2	3	4	6	11	17	5

All-Hadronic Fits

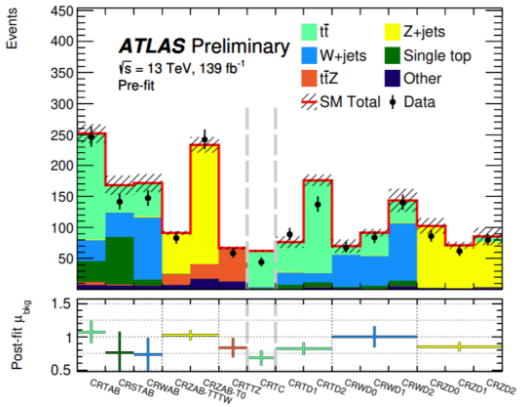

Figure 8: A summary of the normalisation factors determined from the various background-only fits. The total number of data events (points) and the SM expectation (stacked histograms) are shown in each control region before the fit. The uncertainty associated with the SM expectation includes the combination of MC statistical uncertainties, theory-related and detector-related systematic uncertainties. The normalisation factor applied to each background source (μ_{bkg}) after the fit and respective uncertainty, including the combination of MC statistical uncertainties, theory-related and detector-related systematic uncertainties, is shown in the lower panel. The control regions included in the SRA–B, SRC and SRD fits are separated by vertical dashed lines.

Table 14: Left to right: 95% CL upper limits on the visible cross section ($\langle\epsilon\sigma\rangle^{95}_{\text{obs}}$) and on the number of signal events (S^{95}_{obs}). The third column (S^{95}_{exp}) shows the 95% CL upper limit on the number of signal events, given the expected number (and $\pm1\sigma$ excursions on the expectation) of background events. The last two columns indicate the CL_B value, i.e. the confidence level observed for the background-only hypothesis, the discovery p-value ($p(s = 0)$), and the significance (Z).

Signal Region	$\langle\epsilon\sigma\rangle^{95}_{\text{obs}}$[fb]	$S_{\text{obs}^{95}}$	S^{95}_{exp}	CL_B	p(s = 0) (Z)
SRA-TT	0.04	6.0	$5.2^{+2.7}_{-1.7}$	0.63	0.34 (0.40)
SRA-TW	0.06	8.6	$6.5^{+3.2}_{-1.6}$	0.78	0.18 (0.92)
SRA-T0	0.05	6.4	10^{+5}_{-3}	0.11	0.50 (0.00)
SRA-TT-Disc	0.06	8.4	9^{+4}_{-2}	0.39	0.50 (0.00)
SRB-TT	0.28	38.5	22^{+9}_{-6}	0.95	0.03 (1.87)
SRB-TW	0.21	28.6	27^{+10}_{-7}	0.57	0.42 (0.19)
SRB-T0	0.51	71.1	60^{+22}_{-16}	0.69	0.30 (0.53)
SRC1	0.19	26.0	22^{+4}_{-9}	0.75	0.49 (0.01)
SRC2	0.24	32.8	27^{+10}_{-7}	0.76	0.22 (0.77)
SRC3	0.17	24.0	20^{+7}_{-5}	0.76	0.23 (0.75)
SRC4	0.06	8.0	9^{+4}_{-2}	0.29	0.50 (0.00)
SRC5	0.05	6.6	$5.0^{+2.8}_{-1.2}$	0.73	0.22 (0.78)
SRC-Disc	0.11	15.4	15^{+6}_{-4}	0.53	0.49 (0.02)
SRD0	0.04	5.4	$6.8^{+3.3}_{-2.1}$	0.28	0.50 (0.00)
SRD1	0.04	6.2	$5.5^{+2.7}_{-1.8}$	0.63	0.34 (0.40)
SRD2	0.05	6.9	8^{+4}_{-2}	0.28	0.50 (0.00)

Semi-Leptonic Stop

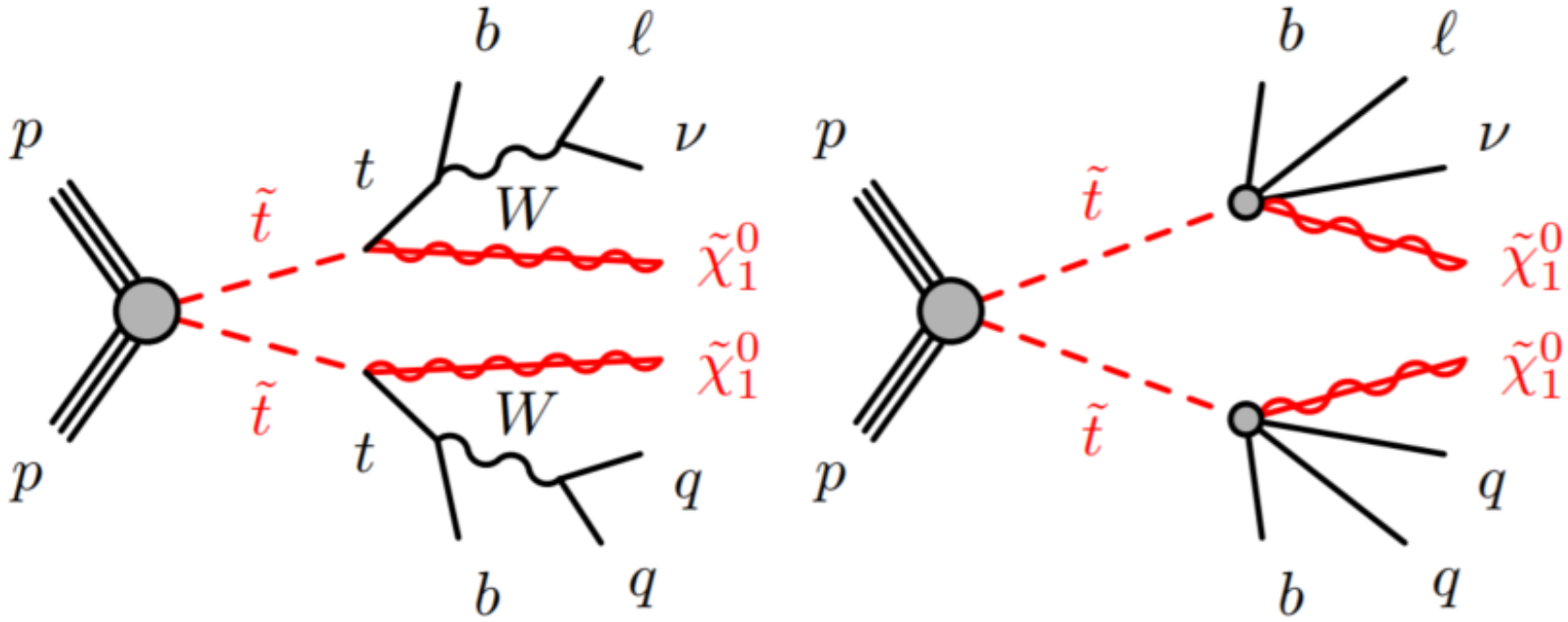

Figure 1: Diagrams illustrating the stop decay modes, which are referred to as (left) $\tilde{t}_1 \to t + \tilde{\chi}_1^0$ and (right) $\tilde{t}_1 \to bff'\tilde{\chi}_1^0$. Sparticles are shown as red lines. In these diagrams, the charge-conjugate symbols are omitted for simplicity. All considered processes involve the production of a squark–antisquark pair.

LSP = lightest neutralino ($\tilde{\chi}_1^0$), interpreted as DM

Two-body dominate when $\Delta m_{\tilde{t},\tilde{\chi}_1^0} > m_{\text{top}}$, four-body dominate at small values of $\Delta m_{\tilde{t},\tilde{\chi}_1^0}$

Semi-Leptonic Region Definitions

Signal region

Selection		DM_scalar	DM_pseudo
Preselection		hard-lepton preselection	
N_{jet}, $N_{b\text{-jet}}$		$\geq (4, 2)$	
Jet p_{T}	[GeV]	$> (80, 60, 30, 25)$	
b-tagged jet p_{T}	[GeV]	$> (80, 25)$	
$E_{\text{T}}^{\text{miss}}$	[GeV]	> 230	
$H_{\text{T,sig}}^{\text{miss}}$		> 15	
m_{T}	[GeV]	> 180	
topness		> 8	
$m_{\text{top}}^{\text{reclustered}}$	[GeV]	> 150	
$\Delta\phi(\text{jet}_i, \vec{p}_{\text{T}}^{\text{miss}})$, $i \in [1, 4]$	[rad]	> 0.9	
$\Delta\phi(\vec{p}_{\text{T}}^{\text{miss}}, \ell)$	[rad]	> 1.1	> 1.5
Exclusion technique		Based on shape fit in $\Delta\phi(\vec{p}_{\text{T}}^{\text{miss}}, \ell)$	
Bin boundaries in $\Delta\phi(\vec{p}_{\text{T}}^{\text{miss}}, \ell)$		$\{1.1, 1.5, 2.0, 2.5, \pi\}$	

Control region

Selection		DM	DM-TCR (-TVR)
$m_{\text{top}}^{\text{reclustered}}$	[GeV]	> 150	veto (> 150)
$H_{\text{T,sig}}^{\text{miss}}$		> 15	> 13 (> 15)
topness		> 8	< 8
$\Delta\phi(\text{jet}_i, \vec{p}_{\text{T}}^{\text{miss}})$	[rad]	> 0.9	> 0.6

Topness Variable

To reject dileptonic $t\bar{t}$ backgrounds where one lepton is lost, *topness* is used

Tests how well an event can be reconstructed under a dileptonic top hypothesis using a likelihood method, including permutations of b-jets (if event has more than one)

$$\mathcal{S}(p_{W_x}, p_{W_y}, p_{W_z}, p_{\nu_z}) = \frac{(m_W^2 - p_W^2)^2}{a_W^4} + \frac{(m_t^2 - (p_{b1} + p_\ell + p_\nu)^2)^2}{a_t^4} + \frac{(m_t^2 - (p_{b2} + p_W)^2)^2}{a_t^4} + \frac{(4m_t^2 - (\Sigma_i p_i)^2)^2}{a_{CM}^4}$$

Minimization with respect to p_W and p_ν where $\vec{p}_{T,\nu} + \vec{p}_{T,W} = \vec{p}_T^{\,\text{miss}}$

Semi-Leptonic Systematics

Table 12: Summary of the dominant systematic uncertainties in % of the total predicted background yields in the SRs, obtained from the background-only fits described in Section 10.

SR Uncertainty (%)	tN_med	tN_high	tN_diag_low	tN_diag_high	bffN_btag	bffN_softb	DM
$t\bar{t}$ normalisation	4.4	2.7	12.3	15.8	6.6	3.7	2.1
$t\bar{t}+Z$ normalisation	9.0	6.8	–	–	–	–	8.0
W+jets normalisation	3.0	4.8	–	–	5.5	11.1	–
Wt normalisation	2.8	3.4	–	–	–	–	–
$t\bar{t}$ modelling	3.0	9.1	18.4	29.3	3.1	3.3	6.1
$t\bar{t}+Z$ modelling	7.7	7.1	–	–	–	–	3.3
W+jets modelling	2.3	3.8	–	–	4.3	9.7	–
Wt modelling	0.5	0.8	–	–	–	–	4.2
JER	10.9	5.1	4.1	5.0	1.8	7.6	8.3
$E_{\mathrm{T}}^{\mathrm{miss}}$ experimental	0.7	0.4	1.0	0.2	2.4	3.4	1.9
b-tagging experimental	1.7	3.6	1.3	0.9	1.9	3.2	4.2
JES	6.0	2.5	4.7	4.1	6.1	11.7	2.5
Leptons experimental	1.0	1.6	1.3	0.3	2.3	4.9	1.2
Pile-up	1.1	1.2	1.2	0.3	1.0	2.1	1.4
Theory	0.9	1.3	1.4	0.5	3.8	3.7	1.1
Monte Carlo statistics	4.1	6.6	5.8	3.5	4.9	17.2	3.2
Total	19	17	24	33	20	27	23

Semi-Leptonic Fit

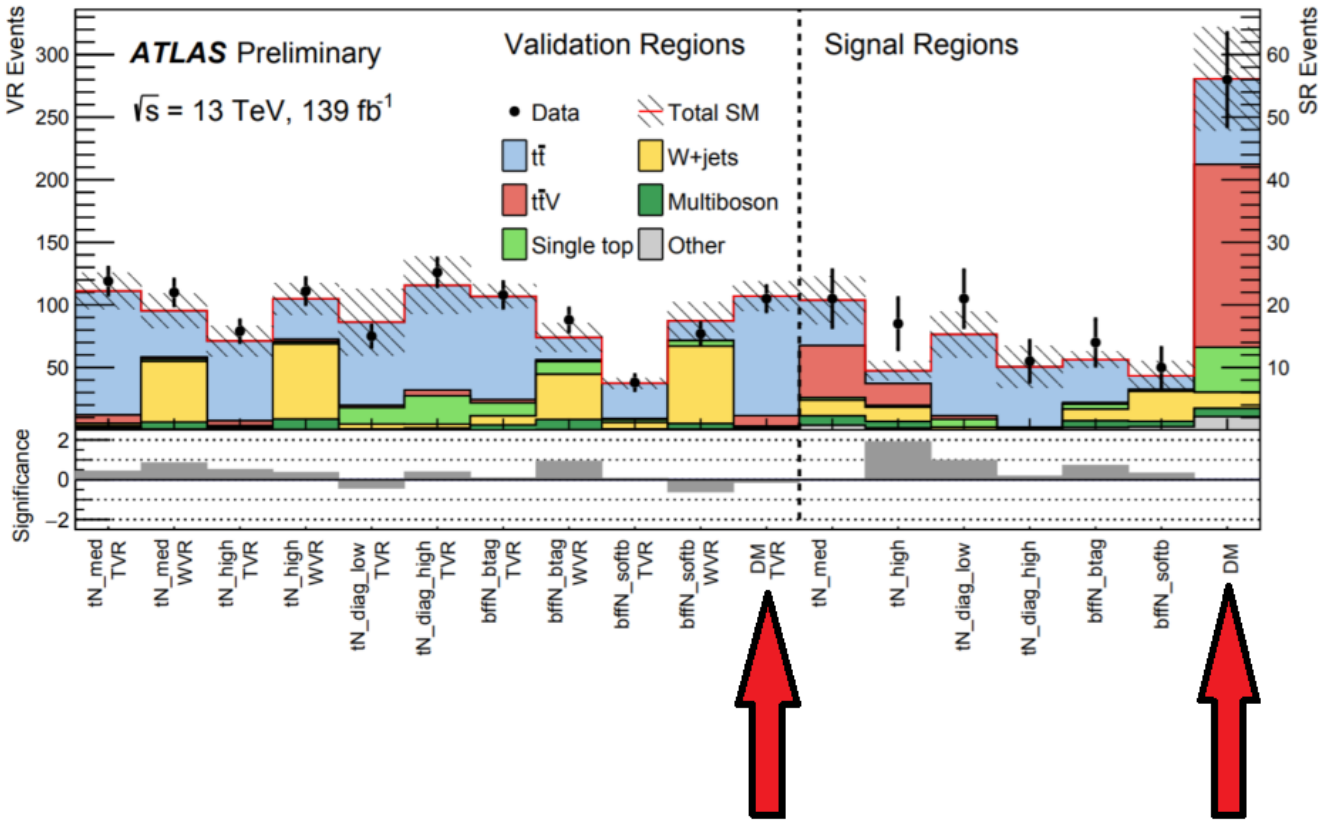

Background-only fit to normalize backgrounds, Z significance shown in bottom plot SRs not orthogonal ⇒ not statistically independent

Other featured analyses

Dark Photon Models

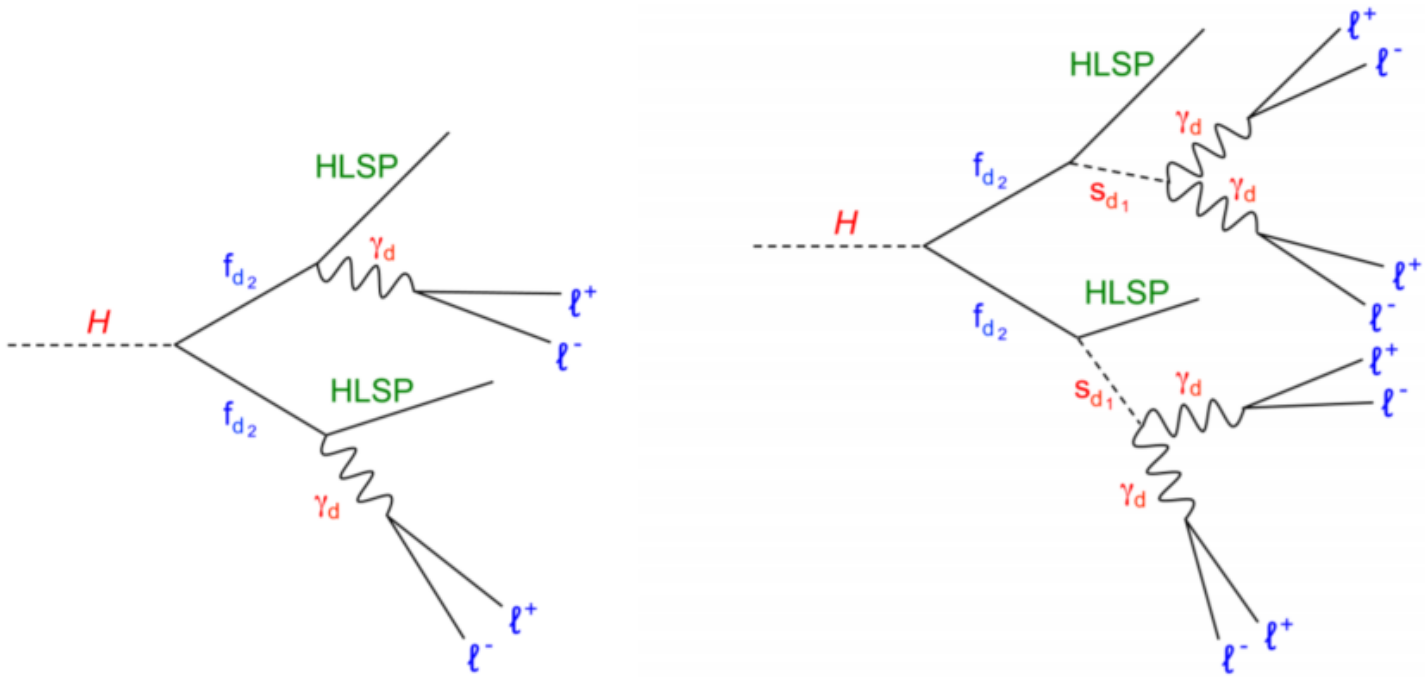

Figure 14: Diagrams of the Higgs portal model with dark photon final states. The dark fermions f_{d_2} each decay into a HLSP and a dark photon γ_d in the diagram on the left, and a HLSP and a dark scalar s_d that in turn decays into a pair of γ_d in the diagram on the right. The γ_d decay into SM fermions, denoted by ℓ^+ and ℓ^-.

RECAST re-analysis of displaced jets in hadronic calorimeter compared to search for collimated leptons or light hadrons

Dark Photon Constraints

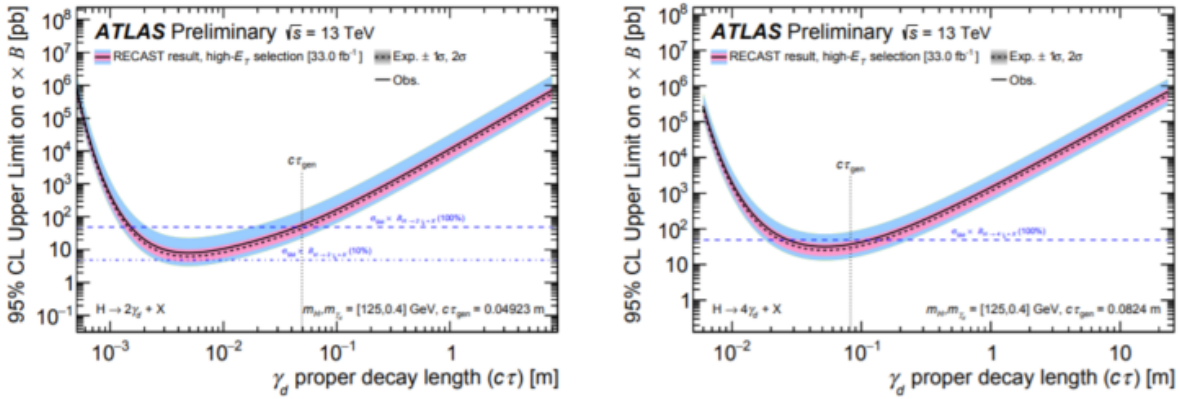

(a) $m_H = 125$ GeV

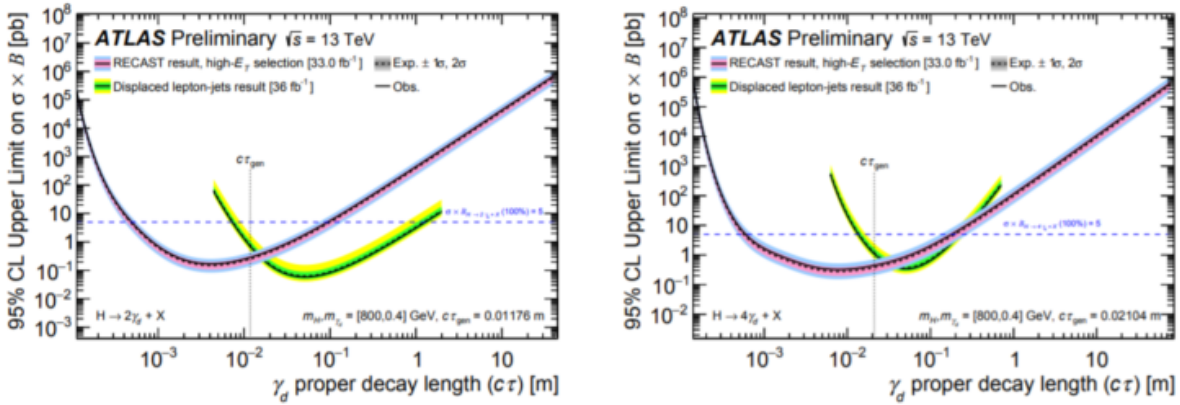

(b) $m_H = 800$ GeV

Figure 16: The constraints from the newly preserved CalRatio jet analysis [5] (compared to those in Ref. [41] for the hDPJ-hDPJ selection, where applicable) for two values of m_H for the two dark photon final state (left) and the four dark photon final state (right). The dashed blue lines indicate $\sigma_H \times B_{H\to N\gamma_d+X}$ with 100% or 10% branching ratios and the SM Higgs gluon-gluon fusion production cross-section $\sigma_H = 48.58$ pb [35] assumed for $m_H = 125$ GeV, and $\sigma_H \times B_{H\to N\gamma_d+X}(100\%) = 5$ pb assumed for $m_H = 800$ GeV.

Higgs-Portal Baryogenesis

- RECAST re-analysis of displaced hadronic jets for 125 GeV Higgs
- Decays violate lepton/boson conservation
- Reanalysis extends lower limits on top of previous work with jets displaced in muon spectrometer

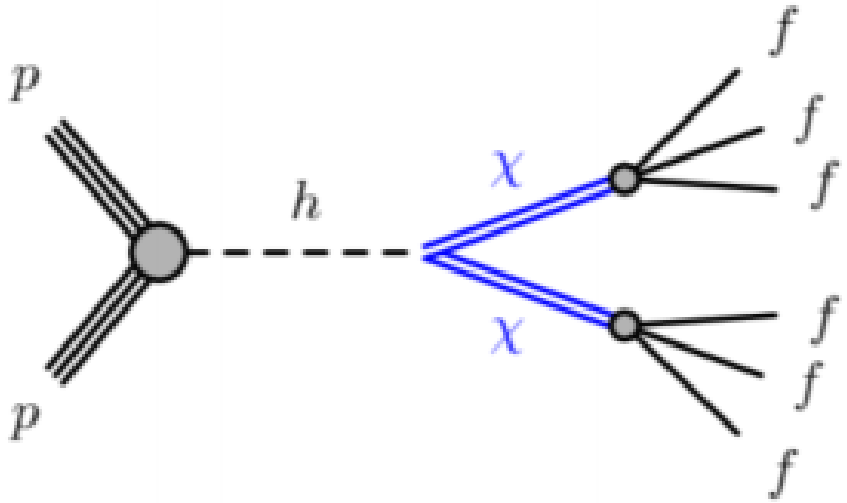

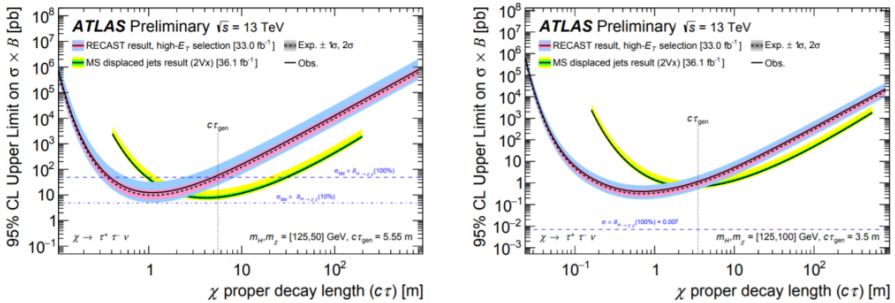

Figure 13: A comparison of the constraints from the high-E_T dataset of the newly preserved CalRatio jet analysis [5] (pink/blue) and the results in Ref. [28] (green/yellow) for the $\chi \to \tau\tau\nu$ decay mode of the Higgs-portal baryogenesis model. The dashed blue lines indicate $\sigma_h \times B_{h\to\chi\chi}$ with 100% or 10% branching ratios and the SM Higgs gluon-gluon fusion production cross-section $\sigma_h = 48.58$ pb [35] assumed for on-shell χ production, and $\sigma_h \times B_{h\to\chi\chi}(100\%) = 0.007$ pb assumed for off-shell production ($m_\chi = 100$ GeV).

Gluino/LSP Production

R-parity conserving SUSY models provide DM candidate in LSP ($\tilde{\chi}_1^0$).
R-parity violating models are also considered in this search (Fig. c)

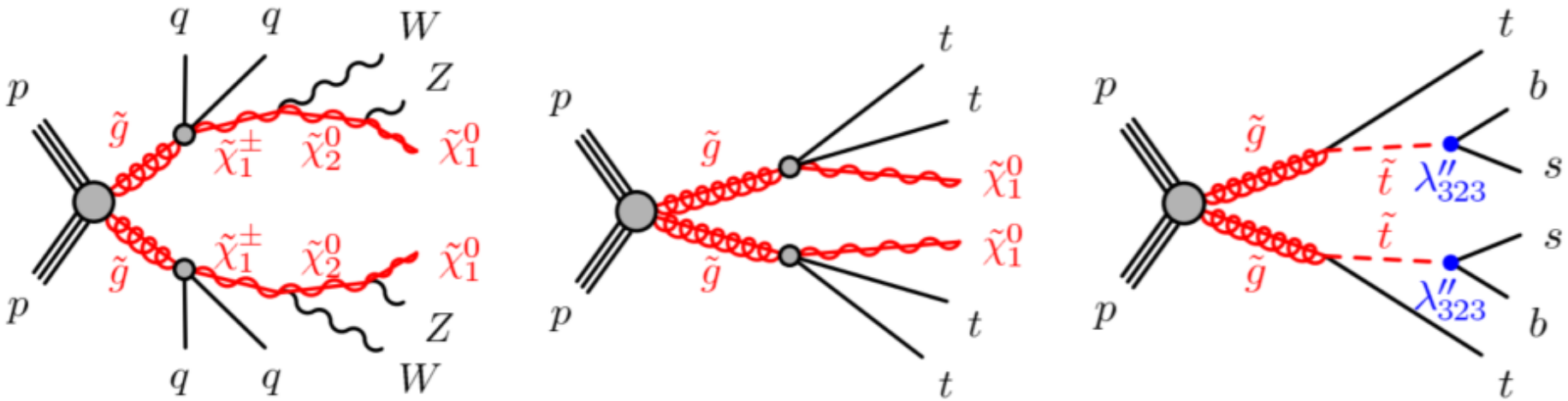

(a) Two-step decay (b) Off-shell top squarks (c) RPV

Figure 1: Pseudo-Feynman diagrams for the different signal models used in this search. λ''_{323} in (c) is one of the couplings of the third generation squark to quarks in the RPV model.

Gluino/LSP Regions

$$M_J^{\Sigma} = \sum_j m_j^{R=1.0}$$

$$\mathcal{S}(E_T^{miss}) = \frac{E_T^{\text{miss}}}{\sqrt{\sigma_L^2(1-\rho_{LT}^2)}}$$

Signal region	N_{jet}^{50}	$N_{b\text{-jet}}$	M_J^{Σ} (GeV)
SR-8ij50 multi-bin	≥8	= 0, = 1, ≥ 2	(0, 340], (340, 500], (500, ∞)
SR-9ij50 multi-bin	≥9		
SR-10ij50 multi-bin	≥10		

Table 2: Signal region subdivisions for the multi-bin fit in the {8,9,10}ij50 analysis channels. The sele these variables apply to the signal regions as well as to the multijet template and validation regions describ Section 6. For each inclusive jet multiplicity fit, nine regions are generated combining the $N_{b\text{-jet}}$ and M_J^{Σ} s

Signal region	N_{jet}^{50}	N_{jet}^{80}	$N_{b\text{-jet}}$	M_J^{Σ} (GeV)
SR-8ij50-0ib-MJ500	≥8	-	-	≥500
SR-9ij50-0ib-MJ340	≥9	-	-	≥340
SR-10ij50-0ib-MJ340	≥10	-	-	≥340
SR-10ij50-0ib-MJ500	≥10	-	-	≥500
SR-10ij50-1ib-MJ500	≥10	-	≥1	≥500
SR-11ij50	≥11	-	-	-
SR-12ij50-2ib	≥12	-	≥2	-
SR-9ij80	-	≥9	-	-

Table 3: Summary of signal region criteria for single-bin selections. The requirements in multiplicity an inclusive in all cases. A dash ('-') indicates that there is no requirement applied to the corresponding vari requirement $\mathcal{S}(E_{\text{T}}^{\text{miss}}) > 5$ is applied to all bins.

N_{jet}^{50}	N_{jet}^{80}	$\mathcal{S}(E_{\text{T}}^{\text{miss}})$ selection
≥8	–	>5
≥9	–	>4
≥10, ≥11	≥8	>4

Table 6: Summary of the individual $\mathcal{S}(E_{\text{T}}^{\text{miss}})$ selections for the leptonic control regions.

Selection criterion	Selection ranges
Lepton multiplicity	Exactly one signal e or μ remaining after overlap removal
Lepton p_{T}	> 20 GeV
m_{T} (ℓ,$E_{\text{T}}^{\text{miss}}$)	< 120 GeV
Trigger	Same as signal regions
Jet p_{T}, $\lvert\eta\rvert$	Same as signal regions
N_{jet} (including lepton)	≥ 8, for N_{jet}^{50} ≥ 8 signal regions; ≥ ($N_{\text{jet}}^{\text{SR}}$ − 1), otherwise
$N_{b\text{-jet}}$	= 0 (WCR), ≥ 1 (TCR)
M_J^{Σ}	Same as signal regions
$\mathcal{S}(E_{\text{T}}^{\text{miss}})$	Table 6

Table 7: Summary of the selections used to define the leptonic control regions.

8, 9, 10ij50 CR definitions	$N_{b\text{-jet}} = 0$	$N_{b\text{-jet}} \geq 1$
$M_J^{\Sigma} \leq 340$ GeV	WCR1	TCR1
340 GeV < $M_J^{\Sigma} \leq 500$ GeV	WCR2	TCR2
$M_J^{\Sigma} > 500$ GeV	WCR3	TCR3

Table 8: Control region subdivisions for the background fits for multi-bin signal selections.

Gluino Multijet Background Estimation

- Multijet Template Estimate defines template regions (in jet multiplicity and $\mathcal{S}(E_T^{miss})$) to estimate contribution from data
- $\mathcal{S}(E_T^{miss})$ independent of jet multiplicity
- Leptonic backgrounds subtracted from Template Regions
- Bin in H_T to eliminate secondary dependence on event kinematics
  - Introduce MJ non-closure uncertainty

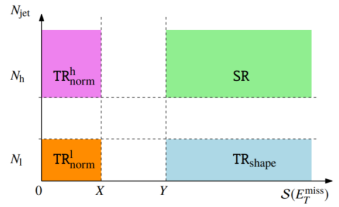

Figure 2: Schematic of the kinematic regions used in the template method for the multijet background. SR represents any signal region, while the three TR variations are regions used to extract and normalise the corresponding background prediction.

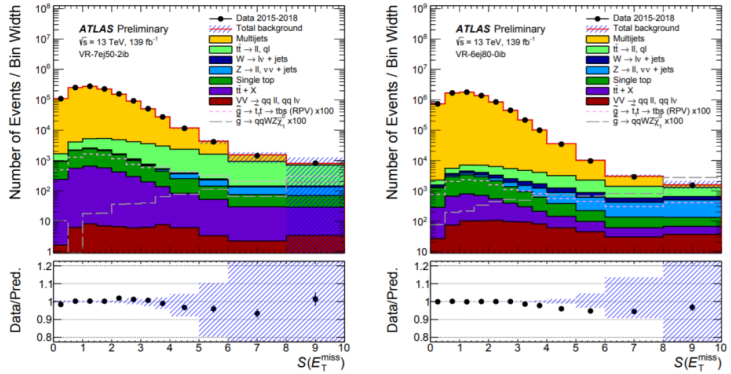

(a) $N_{jet}^{50} = 7$, $N_{b\text{-jet}} \geq 2$ (b) $N_{jet}^{80} = 6$, $N_{b\text{-jet}} \geq 0$

Figure 3: Distributions of the $\mathcal{S}(E_T^{miss})$ for events in two of the validation regions. The upper panel shows the absolute yields for data (black points) and all background subcomponents (histograms), with the combination of statistical and systematic uncertainties shown by the hatched areas. The yields for two benchmark signal models are overlaid, representing 1.6 TeV gluinos decaying to W and Z bosons and a 100 GeV neutralino via intermediate gauginos (long dashed histogram) or instead to tbs/tbd via a 600 GeV top squark through an R-parity violating (RPV) coupling (short dashed histogram). Signal yields have been scaled by a factor of 100 for visibility. The lower panel shows the ratio of the data yields to the total SM prediction.

$\mathcal{S}(E_T^{miss})$ range	0-2	2-3	3-4	4-5	> 5
$N_{jet}^{50} = 6$, prescaled data	$TR^{l,prescale}_{norm}$	–	–	–	$TR^{prescale}_{shape}$
$N_{jet}^{50} = 7$, full dataset	$TR^{h,prescale}_{norm}$	–	–	–	$VR_{N_{jet}}$
$N_{jet}^{50} = 7$, full dataset	TR^{l}_{norm}	–	–	–	TR_{shape}
$N_{jet}^{50} \geq 8$, full dataset	TR^{h}_{norm}	–	QCR	$VR_{\mathcal{S}(E_T^{miss})}$	SR

Table 5: Illustration of the main multijet template, control and validation regions in N_{jet} and $\mathcal{S}(E_T^{miss})$ corresponding to the `j50` signal regions. The template regions needed to derive predictions in the control and $VR_{\mathcal{S}(E_T^{miss})}$ regions are not shown. For the rows labeled "prescaled data", a six-jet trigger was used that collected only a fraction of the Run 2

Gluino Fit

Backgrounds other than data-driven multijet and low contributions taken directly from MC are computed from background-only fits to control regions

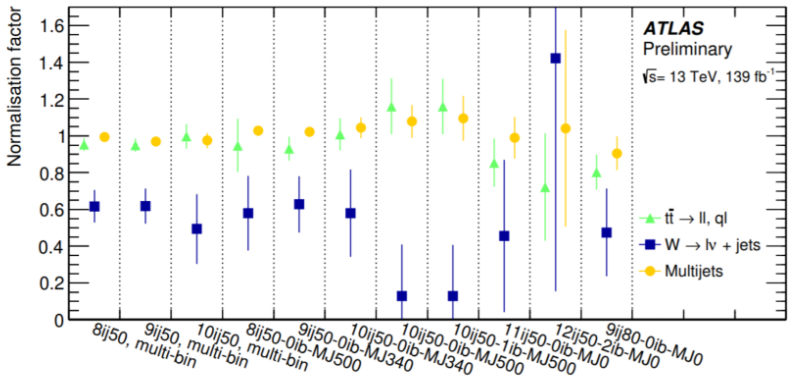

Figure 5: Summary of the fitted normalisation factors for the $t\bar{t}$, W+jets and multijet backgrounds in all signal regions. The error bars indicate the combination of statistical and systematic uncertainties on the corresponding factors. Two pairs of SRs, namely the `SR-8ij50` and `SR-9ij50` multi-bin regions and the `SR-10ij50-0ib-MJ500` and `SR-10ij50-1ib-MJ500` single-bin regions share leptonic control regions, and therefore have highly correlated normalisation factors for the W+jets and $t\bar{t}$ background components.

Signal region	Total syst.	Dominant systematic uncertainties					
`SR-8ij50-0ib-MJ500`	16%	$E_{\mathrm{T}}^{\mathrm{miss}}$ soft, L	7%	$E_{\mathrm{T}}^{\mathrm{miss}}$ soft, T	7%	Z+jets PS	5%
`SR-9ij50-0ib-MJ340`	16%	$E_{\mathrm{T}}^{\mathrm{miss}}$ soft, T	9%	$E_{\mathrm{T}}^{\mathrm{miss}}$ soft, L	9%	Z+jets PS	4%
`SR-10ij50-0ib-MJ340`	20%	$t\bar{t}$ FSR	9%	MC stat.	9%	$E_{\mathrm{T}}^{\mathrm{miss}}$ soft, L	8%
`SR-10ij50-0ib-MJ500`	27%	$t\bar{t}$ FSR	17%	MC stat.	12%	$E_{\mathrm{T}}^{\mathrm{miss}}$ soft, L	9%
`SR-10ij50-1ib-MJ500`	24%	MC stat.	14%	$E_{\mathrm{T}}^{\mathrm{miss}}$ soft, L	10%	$E_{\mathrm{T}}^{\mathrm{miss}}$ soft, T	10%
`SR-11ij50`	27%	MC stat.	18%	$t\bar{t}$ FSR	14%	$t\bar{t}$ norm	6%
`SR-12ij50-2ib`	70%	MC stat.	62%	MJ norm	25%	MJ H_{T} binning	13%
`SR-9ij80`	21%	MC stat.	14%	Z+jets PS	14%	Z+jets match	7%
`SR-8ij50 multi-bin`	6%	MJ closure	3%	JES flavour	3%	JES flavour	2%
`SR-9ij50 multi-bin`	7%	MJ closure	4%	Z+jets PS	3%	$E_{\mathrm{T}}^{\mathrm{miss}}$ soft, L	3%
`SR-10ij50 multi-bin`	14%	Z+jets PS	6%	MJ closure	6%	$t\bar{t}$ FSR	5%

Table 9: The total systematic uncertainties are shown for each of the single-bin signal regions, and also for the multi-bin signal regions, together with the three dominant contributions for each. The individual uncertainties can be (anti-)correlated, and do not necessarily sum quadratically to the total background uncertainty. For the multi-bin signal regions the uncertainties are those found after summing the expected yields over the corresponding M_{J}^{Σ} and b-jet multiplicity bins of Table 2. Within the table 'MC stat.' indicates the statistical uncertainty on simulated events in the SR, 'MJ' indicates the uncertainty on the multijet background, 'closure' indicates the uncertainty from the multijet template method closure, 'norm' is the result of statistical uncertainties from the CRs, 'JES flavour' indicates the uncertainties on the jet energy scale due to differences between quark- and gluon-initiated jets, '$E_{\mathrm{T}}^{\mathrm{miss}}$ soft, L/T' indicate two sources, longitudinal and transverse, of uncertainty on the soft component of the missing transverse momentum, 'MJ H_{T} binning' relates to the parameters of the binning of the multijet template in H_{T}, 'FSR' indicates final state radiation, 'match' indicates the matrix element/parton shower matching scale, and 'PS' is the uncertainty from varying the scale at which the strong coupling constant is calculated for parton shower emissions in the MC calculation.